

Supplementary Materials for

Different genetic barriers for resistance to HA stem antibodies in influenza H3 and H1 viruses

Nicholas C. Wu*, Andrew J. Thompson*, Juhye M. Lee, Wen Su, Britni M. Arlian, Jia Xie,
Richard A. Lerner, Hui-Ling Yen, Jesse D. Bloom, Ian A. Wilson†

*These authors contributed equally to this work.

†Corresponding author. Email: wilson@scripps.edu

Published 19 June 2020, *Science* **368**, 1335 (2020)

DOI: 10.1126/science.aaz5143

This PDF file includes:

Materials and Methods

Figs. S1 to S12

Tables S1 to S3

References

31 **Materials and Methods**

32 **Cell cultures**

33 HEK293T cells and MDCK-SIAT1 cells (Sigma-Aldrich) were maintained in DMEM medium
34 (Thermo Fisher Scientific) supplemented with 10% fetal bovine serum (Thermo Fisher
35 Scientific), 1x MEM non-essential amino acids (Thermo Fisher Scientific) and 100 U mL⁻¹ of
36 Penicillin-Streptomycin (Thermo Fisher Scientific). Madin-Darby Canine Kidney (MDCK) cells
37 and Vero cell lines were maintained in minimal essential medium (MEM) containing 10% fetal
38 bovine serum and 1% Penicillin-Streptomycin. Human embryonic kidney 293T cells were
39 maintained in Opti-MEM I reduced serum media containing 5% fetal bovine serum and 1%
40 Penicillin-Streptomycin. MDCK-SIAT1-TMPRSS2 cells (38) were maintained in DMEM
41 supplemented with 10% heat-inactivated fetal bovine serum, 2 mM L-glutamine, 100 U mL⁻¹ of
42 Penicillin, and 100 μ g mL⁻¹ of Streptomycin. Sf9 cells (ATCC) and High Five cells (Thermo
43 Fisher Scientific) were maintained in HyClone insect cell culture medium (GE Healthcare), and
44 Expi293F cells (Thermo Fisher Scientific) in Expi293 expression medium (Thermo Fisher
45 Scientific).

46

47 **Influenza virus**

48 H3N2 A/Hong Kong/1/1968 (H3/HK68)

49 H3/HK68 virus was generated using a chimeric approach as described previously where the HA
50 and NA were derived from H3N2 A/Hong Kong/68 virus and the other influenza proteins from
51 H1N1 A/WSN/33 virus (30). Briefly, chimeric H3/HK68 HA was constructed based on the
52 pHW2000 plasmid (50) that encodes the HA ectodomain (1_{HA1} to 175_{HA2} , H3 numbering) from
53 A/Hong Kong/1/1968 flanked by the 32-nucleotide 3' non-coding region plus the coding region
54 for the 19 amino acids of the signal peptide from H1/WSN HA at the N terminus, and the coding
55 region for the 46 amino acids of the transmembrane domain and cytoplasmic tail plus 48-
56 nucleotide 5' non-coding region from H1/WSN HA at the C terminus (30). For the NA segment,
57 the entire coding region of full-length N1/WSN NA was replaced with that of N2/HK68 NA, with
58 the non-coding regions from N1/WSN. For virus rescue experiments, transfection was
59 performed in HEK293T/MDCK-SIAT1 cells co-culture (ratio of 6:1) using lipofectamine 2000
60 (Thermo Fisher Scientific) according to the manufacturer's instructions. Virus rescue
61 experiments for H3/HK68 (WT, mutant, or mutant libraries) were performed with the HA and NA
62 segments described above, and the other six WT gene segments from H1/WSN. At 24 hours
63 post-transfection, cells being washed twice with PBS (Thermo Fisher Scientific) and cell culture
64 media were replaced with OPTI-MEM medium (Thermo Fisher Scientific) supplemented with
65 $0.8 \mu\text{g mL}^{-1}$ TPCK-trypsin (Thermo Fisher Scientific). Virus was harvested at 72 hours post-
66 transfection. MDCK-SIAT1 cells were used for titering and infection, cells were washed twice
67 with PBS prior to the addition of virus, and OPTI-MEM medium supplemented with $0.8 \mu\text{g mL}^{-1}$
68 TPCK-trypsin was used.

69

70 To generate recombinant H3/HK68 (7:1 on H1/PR8 backbone) viruses, chimeric H1/PR8-
71 flanked H3/HK68 HA was constructed based on the pHW2000 plasmid (50) that encodes the
72 HA ectodomain (1_{HA1} to 175_{HA2} , H3 numbering) from A/Hong Kong/1/1968 flanked by the 32-
73 nucleotide 3' non-coding region and the coding region for the 19 amino acids of the signal
74 peptide from H1/PR8 HA at the N terminus, and the coding region for the 46 amino acids of the

75 transmembrane domain and cytoplasmic tail plus the 48-nucleotide 5' non-coding region from
76 H1/PR8 HA at the C terminus. Virus rescue experiments for H3/HK68 (7:1 on H1/PR8
77 backbone) viruses (WT or mutant) were the same as described above for chimeric H3/HK68
78 virus, except that the HA from chimeric H1/PR8-flanked H3/HK68 and the other seven WT
79 segments from H1/PR8 were used.

80

81 **H3N2 A/Wuhan/359/95 (H3/Wuhan95)**

82 The eight gene segments of the H3/Wuhan95 virus were cloned into the dual promoter
83 pHW2000 vector as described (51, 52). Recombinant H3/Wuhan95 viruses were generated in
84 293T cells using TransIT-LT1 (Mirus). Viruses were passaged twice in MDCK cells containing 1
85 µg/ml TPCK-trypsin at a multiplicity of infection (MOI) of 0.001 and 0.005, respectively. The HA
86 genes of the recombinant viruses after two passages in MDCK cells were RT-PCR amplified
87 and verified by Sanger sequencing.

88

89 **Antibodies**

90 CR9114 Fab, 27F3 Fab, and 27F3 IgG were expressed as previously described (26, 34). For
91 CR9114 IgG expression, the CR9114 heavy and light chains were cloned into pFUSE-CHIg-
92 hG1 and pFUSE2-CLIg-hK respectively. The plasmids were co-transfected into Expi293F cells
93 at 2:1 ratio (light to heavy) using lipofactamine 2000 (Thermo Fisher Scientific) according to
94 manufacturer's instructions. The supernatant was collected at 72 hours post-transfection. All
95 expressed Fabs and IgGs did not contain any affinity tag. Full-length IgG proteins were purified
96 from the supernatant using a protein G column on an ÄKTA™ start (GE Healthcare Life
97 Sciences).

98

99 **Construction of H3/HK68 HA mutant libraries**

100 The HA plasmid mutant libraries were created by ligating a mutant library insert and a PCR-
101 generated vector. The mutant libraries were built based on the pHW2000 plasmid (50) that
102 encoded the chimeric A/Hong Kong/1/1968 (H3/HK68) HA (as described above). Silent
103 mutations were introduced at the codons encoding for HA2 residues 43, 44, 50, and 112. These
104 silent mutations acted as an internal barcode to indicate which codon position was being
105 randomized and allowed us to distinguish randomized codon positions from sequencing errors
106 (53). The names and nucleotide sequences of individual primers that were used in this study for
107 mutant library construction are listed in table S2.

108

109 All PCR reactions were performed using KOD DNA polymerase (EMD Millipore) with 1.5 mM
110 MgSO₄, 0.2 mM of each dNTP (dATP, dCTP, dGTP, and dTTP), and 0.6 μ M of forward and
111 reverse primer according to the manufacturer's instructions. All PCR products were purified by
112 gel extraction using PCR Clean-Up and Gel Extraction Kit (Clontech Laboratories).

113

114 Insert for the single mutant library

115 The single mutant library was generated by two PCRs using the WT plasmid as template. In the
116 first PCR, primers StemLib-42-F, StemLib-45-F, StemLib-46-F, StemLib-47-F, StemLib-48-F,
117 StemLib-49-F, and StemLib-52-F (table S2) were mixed at equal molar ratio and were used as
118 the forward primer, whereas primer StemLib-WT-R (table S2) was used as the reverse primer.
119 In the second PCR, primers StemLib-WT-F and StemLib-111-R were used. The products of the
120 first and second PCRs were mixed at a molar ratio of 7:1 (the product of the first PCR to the
121 product of the second PCR). This mixture was the insert for the single mutant library.

122

123 Insert for the double mutant library

124 The double mutant library was generated by two PCRs using the WT plasmid as template. In
125 the first PCR, primers StemLib-42-F, StemLib-45-F, StemLib-46-F, StemLib-47-F, StemLib-48-
126 F, StemLib-49-F, and StemLib-52-F (table S2) were mixed at equal molar ratio and were used
127 as the forward primer, whereas primer StemLib-111-R (table S2) was used as the reverse
128 primer. In the second PCR, primers StemLib-42/45-F, StemLib-42/46-F, StemLib-42/47-F,
129 StemLib-42/48-F, StemLib-42/49-F, StemLib-42/52-F, StemLib-45/46-F, StemLib-45/47-F,
130 StemLib-45/48-F, StemLib-45/49-F, StemLib-45/52-F, StemLib-46/47-F, StemLib-46/48-F,
131 StemLib-46/49-F, StemLib-46/52-F, StemLib-47/48-F, StemLib-47/49-F, StemLib-47/52-F,
132 StemLib-48/49-F, StemLib-48/52-F, and StemLib-49/52-F (table S2) were mixed at equal molar
133 ratio and were used as the forward primer, whereas primer StemLib-WT-R (table S2) was used
134 as the reverse primer. The products of the first and second PCRs were mixed at a molar ratio of
135 1:3 (the product of the first PCR to the product of the second PCR). This mixture was the insert
136 for the double mutant library.

137

138 Vector generation

139 The vector for the mutant libraries was created by PCR using the WT plasmid as template and
140 primers StemLib-VF and StemLib-VR (table S2).

141

142 Restriction digestion, ligation, and transformation

143 Both the vector and inserts were digested with BsmBI (New England Biolabs). Ligation was
144 performed for each mutant library using T4 DNA ligase (New England Biolabs). The ligated
145 products were transformed into MegaX DH10B T1R Electrocomp cells (Thermo Fisher
146 Scientific). At least one million colonies were collected for each mutant library. Plasmid mutant
147 libraries were purified from the bacteria colonies using Maxiprep Plasmid Purification (Clontech
148 Laboratories).

149

150 **HA deep mutational scanning of H3/HK68**

151 Virus mutant libraries were rescued from the plasmid mutant libraries by transfecting
152 HEK293T/MDCK-SIAT1 cells co-culture (ratio of 6:1) using lipofactamine 2000 (Thermo Fisher
153 Scientific) according to the manufacturer's instructions. Transfection for the single mutant library
154 was performed in a T75 cm² flask, and in a T225 cm² flask for the double mutant libraries. Two
155 independent transfections were performed for each mutant library. Subsequently, four virus
156 mutant libraries were produced, namely replicate 1 and 2 of the single mutant library, and
157 replicate 1 and 2 of the double mutant library. For passaging of each virus mutant library,
158 monolayer MDCK-SIAT1 cells in a T75 cm² flask (for the single mutant library) or in a T225 cm²
159 flask (for the double mutant library) were infected with an MOI of 0.05. At 2 hours post-infection,
160 infected cells were washed three times with PBS followed by the addition of fresh medium. The
161 virus mutant library was harvested at 24 hours post-infection. The harvested virus mutant library
162 was also the post-selection library in this study. For profiling antibody resistance, antibody was
163 added to the media at the indicated concentration throughout the course of infection. The
164 antibody was incubated with the virus mutant library for 1 h at room temperature, before the
165 mixture of antibody-virus mutant library being added to the cells. Each virus mutant library
166 (replicate 1 and 2 of the single mutant library, and replicate 1 and 2 of the double mutant library)
167 was passaged in 5 conditions, namely no antibody, 2 µg mL⁻¹ of CR9114 IgG, 10 µg mL⁻¹ of
168 CR9114 IgG, 0.3 µg mL⁻¹ of FI6v3 IgG and 2.5 µg mL⁻¹ of FI6v3 IgG.

169

170 **HA sequencing library preparation for H3/HK68**

171 Viral RNA was extracted using QIAamp Viral RNA Mini Kit (QIAGEN). The extracted RNA was
172 then reverse transcribed to cDNA using Superscript III reverse transcriptase (Thermo Fisher
173 Scientific). The plasmid mutant libraries or the cDNA from the post-infection viral mutant
174 libraries were amplified by PCR using primers: 5'-CAC TCT TTC CCT ACA CGA CGC TCT
175 TCC GAT CTA CAA GCA GCA GAT CTT AAA AGC-3' and 5'-GAC TGG AGT TCA GAC GTG

176 TGC TCT TCC GAT CTT CTC AAA CAG CTT GTT CAT TTC-3'. A second PCR was performed
177 to add the rest of the adaptor sequence and index to the amplicon using primers: 5'-AAT GAT
178 ACG GCG ACC ACC GAG ATC TAC ACT CTT TCC CTA CAC GAC GCT-3' and 5'-CAA GCA
179 GAA GAC GGC ATA CGA GAT XXX XXX GTG ACT GGA GTT CAG ACG TGT GCT-3'.
180 Positions annotated by an "X" represented the nucleotides for the index sequence:
181 Single mutant library (Plasmid): 5'-GTA GCC-3'
182 Double mutant library (Plasmid): 5'-TAC AAG-3'
183 Single mutant library (no antibody, replicate 1): 5'-TTG ACT-3'
184 Single mutant library (no antibody, replicate 2): 5'-GGA ACT-3'
185 Double mutant library (no antibody, replicate 1): 5'-TGA CAT-3'
186 Double mutant library (no antibody, replicate 2): 5'-GGA CGG-3'
187 Single mutant library (2 µg mL⁻¹ of CR9114 IgG, replicate 1): 5'-CTC TAC-3'
188 Single mutant library (2 µg mL⁻¹ of CR9114 IgG, replicate 2): 5'-GCG GAC-3'
189 Double mutant library (2 µg mL⁻¹ of CR9114 IgG, replicate 1): 5'-TTT CAC-3'
190 Double mutant library (2 µg mL⁻¹ of CR9114 IgG, replicate 2): 5'-GGC CAC-3'
191 Single mutant library (10 µg mL⁻¹ of CR9114 IgG, replicate 1): 5'-CGA AAC-3'
192 Single mutant library (10 µg mL⁻¹ of CR9114 IgG, replicate 2): 5'-CGT ACG-3'
193 Double mutant library (10 µg mL⁻¹ of CR9114 IgG, replicate 1): 5'-CCA CTC-3'
194 Double mutant library (10 µg mL⁻¹ of CR9114 IgG, replicate 2): 5'-GCT ACC-3'
195 Single mutant library (0.3 µg mL⁻¹ of FI6v3 IgG, replicate 1): 5'-GTA GCC-3'
196 Single mutant library (0.3 µg mL⁻¹ of FI6v3 IgG, replicate 2): 5'-TAC AAG-3'
197 Double mutant library (0.3 µg mL⁻¹ of FI6v3 IgG, replicate 1): 5'-TTG ACT-3'
198 Double mutant library (0.3 µg mL⁻¹ of FI6v3 IgG, replicate 2): 5'-GGA ACT-3'
199 Single mutant library (2.5 µg mL⁻¹ of FI6v3 IgG, replicate 1): 5'-TGA CAT-3'
200 Single mutant library (2.5 µg mL⁻¹ of FI6v3 IgG, replicate 2): 5'-GGA CGG-3'
201 Double mutant library (2.5 µg mL⁻¹ of FI6v3 IgG, replicate 1): 5'-CTC TAC-3'

202 Double mutant library ($2.5 \mu\text{g mL}^{-1}$ of FI6v3 IgG, replicate 2): 5'-GCG GAC-3'
203 All final PCR products, except those from FI6v3 selections, were mixed (14 samples total) and
204 submitted for next-generation sequencing using one lane of Illumina MiSeq PE300. The final
205 PCR products from FI6v3 selections were mixed (8 samples total) and submitted for next-
206 generation sequencing using 10% of one lane of Illumina MiSeq PE300.

207

208 **HA deep mutational scanning of H1/SI06 and H1/Mich15**

209 The single mutant libraries of H1/SI06 (A/Solomon Islands/3/2006) and H1/Mich15
210 (A/Michigan/45/2015) were constructed in the same manner as the single mutant library of
211 H3/HK68 (see above). The primers are listed in table S3. Virus mutant libraries of H1/SI06 and
212 H1/Mich15 were rescued with all non-HA segments from H1/WSN. Deep mutational scanning
213 was performed as described for the single mutant library of H3/HK68, except only two passage
214 conditions were used, namely no antibody and $0.3 \mu\text{g mL}^{-1}$ of FI6v3 IgG. Of note, H1 is more
215 sensitive to FI6v3 as compared to H3, so lower concentrations were used in the deep
216 mutational scanning of H1, otherwise the virus would not survive. HA sequencing library for
217 H1/SI06 and H1/Mich15 was prepared as described for H3/HK68, except different primers were
218 used for PCR of plasmid mutant libraries and cDNA. For H1/SI06, the plasmid mutant libraries
219 or the cDNA from the post-infection viral mutant libraries were amplified by PCR using primers:
220 5'-CAC TCT TTC CCT ACA CGA CGC TCT TCC GAT CTC TAT GCT GCG GAC CAA AAA
221 AGC-3' and 5'-GAC TGG AGT TCA GAC GTG TGC TCT TCC GAT CTT CTC ATA CAG ATT
222 CTT CAC ATT-3'. For H1/Mich15, the plasmid mutant libraries or the cDNA from the post-
223 infection viral mutant libraries were amplified by PCR using primers: 5'-CAC TCT TTC CCT ACA
224 CGA CGC TCT TCC GAT CTA TAT GCA GCC GAC CTG AAG AGC-3' and 5'-GAC TGG AGT
225 TCA GAC GTG TGC TCT TCC GAT CTT TTC ATA CAA GTT CTT CAC ATT-3'. The index
226 sequence for the second PCR was as follows:
227 H1/SI06 mutant library (no antibody, replicate 1): 5'-CGT GAT-3'

228 H1/SI06 mutant library (no antibody, replicate 2): 5'-ACA TCG-3'
229 H1/Mich15 mutant library (no antibody, replicate 1): 5'-GCC TAA-3'
230 H1/Mich15 mutant library (no antibody, replicate 2): 5'-TGG TCA-3'
231 H1/SI06 mutant library (0.3 µg mL⁻¹ of FI6v3 IgG, replicate 1): 5'-CAC TGT-3'
232 H1/SI06 mutant library (0.3 µg mL⁻¹ of FI6v3 IgG, replicate 2): 5'-ATT GGC-3'
233 H1/Mich15 mutant library (0.3 µg mL⁻¹ of FI6v3 IgG, replicate 1): 5'-GAT CTG-3'
234 H1/Mich15 mutant library (0.3 µg mL⁻¹ of FI6v3 IgG, replicate 2): 5'-TCA AGT-3'
235 H1/SI06 mutant library (Plasmid): 5'-CTG ATC-3'
236 H1/Mich15 mutant library (Plasmid): 5'-AAG CTA-3'
237 The final PCR products from H1/SI06 and H1/Mich15 selections were mixed (10 samples total)
238 and submitted for next-generation sequencing using 30% of one lane of Illumina MiSeq PE300.
239
240 **HA sequencing data analysis for H3/HK68, H1/SI06, and H1/Mich15**
241 For each paired-end read, the positions of randomized codon were first identified by the internal
242 barcode. A paired-end read would be discarded if the corresponding forward and reverse reads
243 did not match at the internal barcode positions or at the randomized codon. This procedure was
244 not applied when analyzing the mutant libraries of H1/SI06 and H1/Mich15, because an internal
245 barcode was not used in the construction of the mutant libraries of H1/SI06 and H1/Mich15.
246 Each mutation was called by comparing individual paired-end reads to the WT reference
247 sequence. Sequencing data for each library were processed independently. For a mutant *i* in
248 mutant library *n* of sample *t* (in this study, *n* could be the single mutant library or double mutant
249 library, and *t* could be input plasmid library or library that was selected under a specified
250 condition):
251 Occurrence frequency_{*i,n,t*} = (Read count_{*i,n,t*} + 1)/Coverage_{*n,t*}, where Read count_{*i,n,t*} represents the
252 number of read in mutant library *n* of sample *t* that carried mutation *i* and coverage_{*n*} represents
253 the sequencing coverage of the mutant library *n* of sample *t*.

254

255 Similarly, Occurrence frequency_{WT,n,t} = (Read count_{WT,n,t} + 1)/Coverage_{n,t}, where Read count_{WT,n}
256 represents the number of read that matches with the WT sequence in mutant library *n* of sample
257 *t* and coverage_{n,t} represents the sequencing coverage of the mutant library *n* of sample *t*.

258

259 Subsequently, Relative frequency_{i,n,t} = (Occurrence frequency_{i,n,t})/(Occurrence frequency_{WT,n,t}),
260 and Relative fitness_{i,n} = (Relative frequency_{i,n,post-selection})/(Relative frequency_{i,n,plasmid}).

261 Of note, a pseudocount was added to the read count when computing the occurrence frequency
262 to avoid division by zero during the calculations of relative frequency and of relative fitness. For
263 each mutant library, a given mutant would be discarded if the number of reads in the plasmid
264 mutant library were <20 (<0.05% input frequency in the single mutant library and <0.003% input
265 frequency in the double mutant library). The reported relative fitness was computed by
266 averaging the relative fitness between replicates.

267 Relative resistance is computed by the ratio between the relative fitness with antibody selection
268 and the relative fitness without antibody selection:

269 Relative resistance_{i,n} = (Relative fitness_{i,n,with antibody})/ (Relative fitness_{i,n,without antibody})
270 Of note, relative resistance values could not be compared between CR9114 and Fl6v3
271 selections since the strengths of selection pressures from CR9114 and Fl6v3 are not
272 normalized in this experiment.

273

274 **Deep mutational scanning of H1/WSN HA and H3/Perth09 HA**

275 The codon-mutant libraries of H1N1 A/WSN/1933 (H1/WSN) HA mutant virus libraries are those
276 described in (37). The codon-mutant libraries of H3N2 A/Perth/16/2009 (H3/Perth09) HA mutant
277 virus libraries are those described in (38). Details of the library generation and sequencing
278 statistics of the mutant libraries can be found in (37, 38).

279

280 We performed antibody selections of the H1/WSN mutant virus libraries with 50 ng mL⁻¹, 70 ng
281 mL⁻¹, and 100 ng mL⁻¹ of CR9114 IgG. We selected the H3/Perth09 mutant virus libraries with 5
282 µg mL⁻¹, 12 µg mL⁻¹, 13 µg mL⁻¹, and 15 µg mL⁻¹ of Fl6v3 IgG. These antibody selection
283 experiments were performed as described previously (23, 31). Briefly, we incubated 10⁶ TCID₅₀
284 per ml of mutant virus library with an equal volume of antibody at the intended concentration at
285 37°C for 1.5 hours. We also included a mock selection control wherein the mutant virus libraries
286 were incubated with Influenza Growth Media (Opti-MEM supplemented with 0.01% heat-
287 inactivated FBS, 0.3% BSA, 100 U mL⁻¹ of penicillin, and 100 µg mL⁻¹ of streptomycin). We used
288 the H1/WSN mutant virus-antibody mixture to infect MDCK-SIAT1 cells, and the H3/Perth09
289 mutant virus-antibody mixture to infect MDCK-SIAT1-TMPRSS2 cells. The media was changed
290 to fresh Influenza Growth Media (as above, except with 0.5% heat-inactivated FBS for the
291 H1/WSN mutant viruses) at two hours post-infection. At 15 hours post-infection, we proceeded
292 with library sequencing preparation.

293

294 We estimated the fraction of the mutant virus libraries surviving antibody selection (i.e. *fraction*
295 *surviving*), as described previously (23). Briefly, we made duplicate 10-fold serial dilutions of the
296 virus libraries to create a standard curve of infectivity. We then performed qPCR of the standard
297 curve and antibody-selected samples using the NP and GAPDH primers provided in (31). We
298 used linear regression to fit a line to relate the logarithm of the viral infectious dose from the
299 standard curve to the difference in Ct values between NP and GAPDH. We then estimated the
300 fraction of each viral library remaining infectious after antibody treatment using this relationship.
301 The fraction of each library that remained infectious ranged from 0.14% to 2.3% for the H1/WSN
302 libraries treated with Fl6v3, 0.17% to 1% for the H1/WSN libraries treated with CR9114, and
303 4.3% to 7.4% for the H3/Perth09 libraries treated with Fl6v3.

304

305 **HA sequencing library preparation for H1/WSN and H3/Perth09**

306 The libraries were prepared for deep sequencing as described in (31, 38). We extracted viral
307 RNA using a Qiagen RNeasy Plus Mini Kit (QIAGEN). The extracted RNA was reverse-
308 transcribed using AccuScript Reverse Transcriptase (Agilent) using H1/WSN HA- or Perth/2009
309 HA-specific primers, provided in (31, 38). Subsequent amplification of the cDNA and Illumina
310 sequencing preparation were performed using a barcoded-subamplicon approach previously
311 described (28, 37). All samples were submitted for next-generation sequencing on both lanes of
312 an Illumina HiSeq 2500 using 2 x 250 bp paired-ends reads in rapid-run mode.

313

314 **HA sequencing data analysis for H1/WSN and H3/Perth09**

315 The dms_tools2 software package (54) (https://jbloomlab.github.io/dms_tools2/, version 2.3.0)
316 was used to analyze the deep sequencing data.

317

318 **Construction of individual HA mutants**

319 Individual mutants for validation experiments were constructed using the QuikChange XL
320 Mutagenesis kit (Stratagene) according to the manufacturer's instructions.

321

322 **Influenza microneutralization assay**

323 Microneutralization assay was performed as previously described (26). Briefly, two-fold serial
324 dilutions of each antibody were incubated with 200 TCID₅₀ for 1 hour. MDCK-SIAT1 cells were
325 washed twice with PBS and inoculated with virus-antibody mixtures. Cytopathic effect (CPE)
326 was recorded at 72 hours post-inoculation. For the microneutralization assay of CR9114 and
327 FI6v3 to H3/HK68, minimum inhibitory concentration (MIC) was the lowest concentration of the
328 antibody that prevented observable CPE.

329

330 **Plaque morphology**

331 Confluent MDCK cells in 6-well plates were infected with 10-fold serial dilutions of virus in 1 ml
332 infection medium for 1 hour. Cells were washed and overlaid with MEM with 0.3% BSA, 0.5%
333 agarose, 1% Penicillin-Streptomycin and 1 µg/ml TPCK-trypsin and incubated at 37°C for 2
334 days. Cells were fixed with 4% formaldehyde overnight and the plaques were visualized by
335 staining with 0.2% crystal violet solution.

336

337 **pH fusion assay**

338 The HA activation pH was determined by syncytium formation in Vero cells. Monolayers of Vero
339 cells were infected with influenza viruses at an MOI of 10 PFU/cell for 1 hour. Six hours after
340 infection, cells were incubated with infection medium containing 5 µg/mL TPCK- trypsin followed
341 by pH adjusted PBS for 5 min at 37°C. Cells were overlaid with MEM containing 5% fetal bovine
342 serum and further incubated at 37°C. When syncytium formation was identified microscopically,
343 the cells were fixed and stained with the Differential Quick Stain Kit (EMS).

344

345 **Analysis of natural amino acid variants**

346 HA protein sequences were downloaded from Influenza Research Database (www.fludb.org/)
347 (32). Sequence alignment was performed by MAFFT version 7.157b (55). HA protein
348 sequences from human H3N2 isolates that were sequenced without any passaging were
349 downloaded from Global Initiative for Sharing Avian Influenza Data (GISAID; <http://gisaid.org>).
350 Passaging history was determined by parsing regular expression in the FASTA header as
351 described previously (33, 56). Sequence logos were generated by WebLogo
352 (<http://weblogo.berkeley.edu/logo.cgi>) (57). A total of 4625 human H3N2 HA sequences, 81
353 human H2N2 HA sequences, and 65 avian H2N2 HA sequences were included in our analysis.
354 For the analysis of human H3N2 sequences, occurrence frequency of each amino acid variant *i*
355 at residue *n* was computed by:

$$\text{occurrence frequency}_{i,n} = \sum_t \frac{\text{occurrence frequency}_{i,n,t}}{\text{Total number of years}}$$

356 where occurrence frequency_{i,n,t} represents the occurrence frequency of amino acid variant *i* at
357 residue *n* in year *t*, and total number of years represents the number of years being sampled. In
358 this case, the total number of years equals 48 (from 1968 to 2015). Calculating occurrence
359 frequency in this manner avoids temporal sampling bias.

360

361 Recombinant HA expression and purification

362 H3/HK68 HAs (WT or mutants) were prepared for binding experiments as previously described
363 (41). Briefly, the ectodomain of HA, which corresponds to 11–329 (HA1) and 1–176 (HA2)
364 based on H3 numbering was fused with an N-terminal gp67 signal peptide and a C-terminal tag
365 consisting of (from N- to C-terminus) BirA biotinylation site, thrombin cleavage site, foldon
366 trimerization domain, and His₆ tag, and cloned into a customized baculovirus transfer vector
367 (41). Recombinant bacmid DNA was generated using the Bac-to-Bac system (Thermo Fisher
368 Scientific). Baculovirus was generated by transfecting purified bacmid DNA into Sf9 cells using
369 FuGene HD (Promega). H1/WSN HA was expressed by infecting suspension cultures of High
370 Five cells with baculovirus at an MOI of 5 to 10 and incubating at 28°C shaking at 110 rpm for
371 72 hours. The supernatant was concentrated. HA0 was purified by Ni-NTA and buffer
372 exchanged into 20 mM Tris-HCl pH 8 and 150 mM NaCl. For binding experiments, HA0 was
373 biotinylated as described (58) and purified by size exclusion chromatography on a Hiload 16/90
374 Superdex 200 column (GE Healthcare) in 20 mM Tris pH 8.0, 150 mM NaCl, and 0.02% NaN3.
375 For crystallization, the HA0 was treated with trypsin (New England Biolabs) to remove the C-
376 terminal tag (BirA biotinylation site, thrombin cleavage site, trimerization domain, and His₆ tag)
377 and to produce the cleaved mature HA (HA1/HA2). The trypsin-digested HA was then purified
378 by size exclusion chromatography on a Hiload 16/90 Superdex 200 column (GE Healthcare) in

379 20 mM Tris pH 8.0, 150 mM NaCl, and 0.02% NaN₃ and concentrated to 9 mg/mL in 10 mM Tris
380 pH 8.0, 50 mM NaCl, and 0.02% NaN₃.

381

382 **Biolayer interferometry binding assay**

383 Binding assay was performed by biolayer interferometry (BLI) using an Octet Red instrument
384 (FortéBio) as described previously (59). Briefly, biotinylated HA0 at 50 µg/mL in 1x kinetics
385 buffer (1x PBS, pH 7.4, 0.01% BSA and 0.002% Tween 20) was loaded onto streptavidin
386 biosensors and incubated with the indicated concentration of Fab or IgG. The assay consisted
387 of five steps: 1) baseline: 60 s with 1x kinetics buffer; 2) loading: 120 s with biotinylated HA0; 3)
388 baseline: 60 s with 1x kinetics buffer; 4) association: 120 s with samples (Fab or IgG); and 5)
389 dissociation: 120 s with 1x kinetics buffer. For estimating the exact K_d, a 1:1 binding model was
390 used. In cases where the binding affinity was relatively weak (K_d > 100 nM), a 1:1 binding model
391 did not fit well due to the contribution of non-specific binding to the response curve.
392 Subsequently, a 2:1 heterogeneous ligand model was used to improve the fitting.

393

394 **Crystallization and structural determination**

395 All H3/HK68 HA mutants were crystallized using the sitting drop vapor diffusion method with 500
396 µL reservoir solution containing 0.1 M sodium cacodylate pH 6.5, 5% PEG 8000, and 38% 2-
397 methyl-2,4-pentanediol. Drops consisting 0.8 µL protein at 10 mg/ml + 0.8 µL precipitant were
398 set up at 20 °C and crystals appeared within 3 days. This crystallization condition was as
399 previously described for H3/HK68 receptor-binding site mutants (30). Diffraction data were
400 collected at the Stanford Synchrotron Radiation Lightsource beamline 12-2 and indexed,
401 integrated, and scaled using HKL2000 (HKL Research) (60). The structure was solved by
402 molecular replacement using Phaser (61) with PDB: 4FNK (58) as the molecular replacement
403 model, then modeled using Coot (62) and refined using Refmac5 (63). Ramachandran statistics

404 were calculated using MolProbity (64). For data collection and refinement statistics, see table
405 S1.

406

407 **Buried surface area calculation**

408 Solvent accessibility was computed by DSSP (65). Buried surface area (BSA) was calculated by
409 subtracting the solvent accessibility of the apo form from that of the bound form. BSA was then
410 normalized to the empirical scale reported in (66) to obtain the relative solvent accessibility
411 (RSA).

412

413 **In vivo pathogenesis and protection study**

414 Male and female 8-to-12-week-old C57BL/6J mice were obtained from The Scripps Research
415 Institute rodent breeding colony and maintained in biosafety containment under pathogen-free
416 conditions. All mouse experiments were approved by The Scripps Research Institute IACUC
417 and complied with recommendations in the Guide for the Care and Use of Laboratory Animals
418 of the National Research Council. All recombinant H3/HK68 (7:1 on H1/PR8 backbone) viruses
419 were grown in MDCK cultures (approximately 40,000,000 cells per virus) for 72 hours in 1x
420 MEM (Invitrogen) supplemented with 0.1% BSA, 1x Penicillin-Streptomycin, 1x L-glutamine
421 (Invitrogen), and 1 μ g ml⁻¹ (final) TPCK-treated trypsin (Sigma). Following incubation,
422 supernatant was collected. Cell debris was pelleted by low-speed centrifugation (500 rcf for 5
423 min), and viruses isolated from the supernatant by high-speed centrifugation at 60,000 rcf. for
424 120 min. Virus pellets were resuspended in sterile 1x PBS containing 5% glycerol, aliquoted,
425 and stored at -80°C. TCID₅₀ titers of all virus stocks were determined in MDCK cell cultures prior
426 to infection studies.

427

428 For pathogenesis experiments, groups of n = 4 or 5 C57BL/6J mice under deep isoflurane
429 anesthesia were inoculated intranasally with 25 μ l doses of H3/HK68 (7:1 on H1/PR8 backbone)

430 WT or mutant viruses, or PBS, ranging from 10^4 to 10^1 TCID₅₀ ml⁻¹. Following infection, mice
431 were monitored for body weight loss or clinical signs of infection every 24 hours up to 15 days
432 post infection. Mice that reached 30% loss of original body weight on day 0, or were observed to
433 have a severe/morbid clinical score on three consecutive days, were humanely euthanized.
434 Resulting data were used to compare infectivity of WT and mutant viral stocks and calculate
435 respective mLD₅₀ titers.

436

437 For prophylactic protection experiments, groups of n = 8 (4 male and 4 female) C57BL/6J mice
438 were intravenously immunized with 100 µl of CR9114 at 10, 4, or 1 mg kg⁻¹ doses, or PBS
439 control, via tail vein injection prior to challenge with a lethal dose of WT or respective mutant
440 H3/HK68 viruses (7:1 on H1/PR8 backbone). 24 hours after immunization, all mice were
441 infected intranasally, exactly as described above, with a dose equivalent to 25 mLD₅₀ of
442 respective virus stocks. All mice were monitored for body weight loss or clinical signs of
443 infection every 24 hours up to 15 days post infection. Mice that reached 30% loss of original
444 body weight on day 0, or were observed to have a severe/morbid clinical score on three
445 consecutive days, were humanely euthanized. Effectiveness of antibody protection was
446 analyzed via Kaplan-Meier survival curves and paired analysis of each treatment group, relative
447 to control, was conducted using Log-rank (Mantel-Cox) tests.

448

449 **Construction of yeast surface display library**

450 The insect cell expression plasmid that encodes WT CR9114 Fab (26) was used as the
451 template to generate the CR9114 Fab yeast display construct. Specifically, the heavy chain and
452 light chain of CR9114 were cloned into the dual promoter yeast expression plasmid that was
453 described previously (59). To construct the insert for the CR9114 mutant library, a PCR was
454 performed using the WT CR9114 Fab yeast expression plasmid as template. The insert was
455 generated using an overlapping PCR strategy with two fragments. The first fragment of the

456 insert was generated using primers: 5'-AAA AGT AGC GGA GGA ACA TCA AAC NNS TAC
457 GCA ATC TCT TGG GTG CGG CA-3' and 5'-CTG AGC GTA GGC TGT ACT CCC MNN SNN
458 SNN AGA GAT CCC GCC CAT CCA GTC-3'. The second fragment of the insert was generated
459 using primers: 5'-GAC TGG ATG GGC GGG ATC TCT NNS NNS NNK GGG AGT ACA GCC
460 TAC GCT CAG-3' and 5'-GAC ATC CAT CCC AGA GTA ATA SNN GTT TCC GTG GCG
461 AGC ACA AAA GT-3'. The two fragments were mixed at equal molar ratio and were used as the
462 template for PCR using primers: 5'-AGC CCG GCA GTA GTG TCA AAG TCA GTT GTA AAA
463 GTA GCG GAG GAA CAT CA-3' and 5'-GAG ACA GTG ACG GTT CCC TGC CCC CAG
464 ACA TCC ATC CCA GAG TAG TA-3'. The product of this overlapping PCR is the insert for the
465 CR9114 mutant library. The vector for the CR9114 Fab mutant library was generated by PCR
466 using the WT CR9114 Fab yeast expression plasmid as template and primers: 5'-TAC TAC TCT
467 GGG ATG GAT GTC TGG GGG CAG GGA ACA ACC GTC ACT GTC TC-3' and 5'-TGA TGT
468 TCC TCC GCT ACT TTT ACA ACT GAC TTT GAC ACT ACT GCC GGG CT-3'. The insert and
469 vector were mixed and transformed into yeast strain EBY100 using a high-efficiency protocol as
470 previously described (67). At least 50 million yeast colonies were collected to generate the
471 CR9114 Fab yeast surface display library, which was resuspended in SDCAA (2.0% glucose,
472 0.67% yeast nitrogen base, 0.5% casamino acids, 0.54% disodium phosphate, 0.86%
473 monosodium phosphate) with 15% glycerol and stored at -80 °C until used.

474

475 **Selection of yeast surface display library**

476 Selection was performed as previously described (59). Briefly, for each round of selection, 10⁹
477 yeast cells from the frozen stock were cultured in 250 mL SDCAA for 16 hours at 28 °C with
478 shaking at 250 rpm. Yeast cells were then pelleted and resuspended in 100 ml SGR-CAA (20 g
479 L⁻¹ galactose, 20 g L⁻¹ raffinose, 1 g L⁻¹ dextrose, 6.7 g L⁻¹ yeast nitrogen base, 5 g L⁻¹
480 casamino acids, 5.4 g L⁻¹ Na₂HPO₄ and 8.56 g L⁻¹ Na₂HPO₄). Yeast cells were cultured for
481 24 hours at 18 °C with shaking at 250 rpm to reach an OD₆₀₀ of 1.2 to 1.6. 8 mL of the yeast

482 culture was spun down, washed twice with PBS, and resuspended in 5 ml PBS. Biotinylated
483 trimeric HA was incubated with streptavidin-PE (eBioscience, San Diego, CA) at a molar ratio of
484 1:4 for 15 min. Of note, Streptavidin PE was buffer exchanged into PBS before use to remove
485 NaN₃, which is toxic to the yeast cells. The biotinylated trimeric HA-streptavidin-PE complex was
486 added to the yeast cells in PBS with a final concentration of 10 nM, or 0.4 nM for round 2 of WT
487 H3/HK68 selection, or 0.016 nM for round 3 of WT H3/HK68 selection. After incubating at 4 °C
488 overnight with head-to-head rotation, the yeast cells were pelleted, washed with PBS,
489 resuspended in 5 mL PBS, and subjected to fluorescence-activated cell sorting (FACS) at TSRI
490 Flow Cytometry Core Facility. The sorted yeast cells were recovered by plating on the SDCAA
491 agar plates. Yeast colonies were collected after 2 days of incubation at 30 °C, resuspended in
492 YPD with 15% glycerol, and stored at -80 °C until used.

493

494 **Next-generation sequencing of yeast surface display library**

495 Plasmid was extracted from at least 10⁷ yeast cells per sample using Zymoprep Yeast Plasmid
496 Miniprep II (Zymo Research) according to the manufacturer's instructions. The mutated region
497 on the CR9114 heavy chain was amplified by PCR using primers: 5'-CAC TCT TTC CCT ACA
498 CGA CGC TCT TCC GAT CTG TAA AAG TAG CGG AGG AAC ATC-3' and 5'-GAC TGG AGT
499 TCA GAC GTG TGC TCT TCC GAT CTC AGA CAT CCA TCC CAG AGT AGT-3'. A second
500 PCR was performed to add the rest of the adaptor sequence and index to the amplicon using
501 primers: 5'-AAT GAT ACG GCG ACC ACC GAG ATC TAC ACT CTT TCC CTA CAC GAC
502 GCT-3' and 5'-CAA GCA GAA GAC GGC ATA CGA GAT XXX XXX GTG ACT GGA GTT CAG
503 ACG TGT GCT-3'. Positions annotated by an "X" represented the nucleotides for the index
504 sequence:

505 Mutant library DNA insert: 5'-CGT GAT-3'

506 Yeast pre-selected mutant library: 5'-ACA TCG-3'

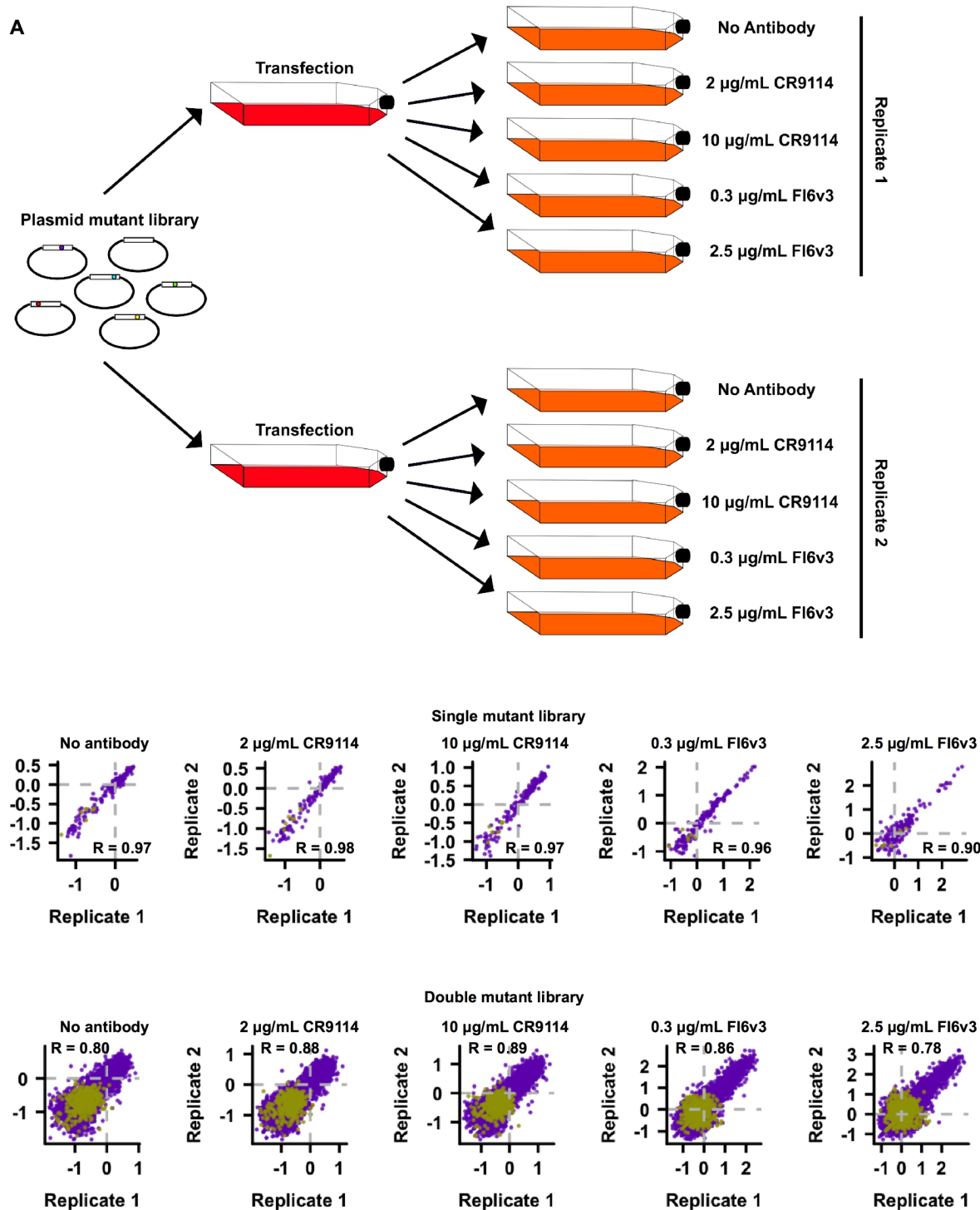
507 WT round 1: 5'-GCC TAA-3'

508 WT round 2: 5'-TGG TCA-3'
509 WT round 3: 5'-CAC TGT-3'
510 I45T round 1: 5'-CTG ATC-3'
511 I45T round 2: 5'-AAG CTA-3'
512 I45T round 3: 5'-GTA GCC-3'
513 I45M round 1: 5'-ATT GCC-3'
514 I45M round 2: 5'-GAT CTG-3'
515 I45M round 3: 5'-TCA AGT-3'
516 I45F round 1: 5'-TAC AAG-3'
517 I45F round 2: 5'-TTG ACT-3'
518 I45F round 3: 5'-GGA ACT-3'
519 For each paired-end read, the nucleotide sequence corresponding to the randomized region
520 was extracted. If the nucleotide sequence at the randomized region was inconsistent between
521 forward and reverse reads, the paired-end read would be discarded. In other words, at the
522 randomized region, the reverse-complement of forward read must perfectly match the reverse
523 read. The nucleotide sequence was translated into the amino-acid sequence. The occurrence of
524 each amino-acid sequence was counted, with each paired-end read as one count.

525

526 **Code availability**

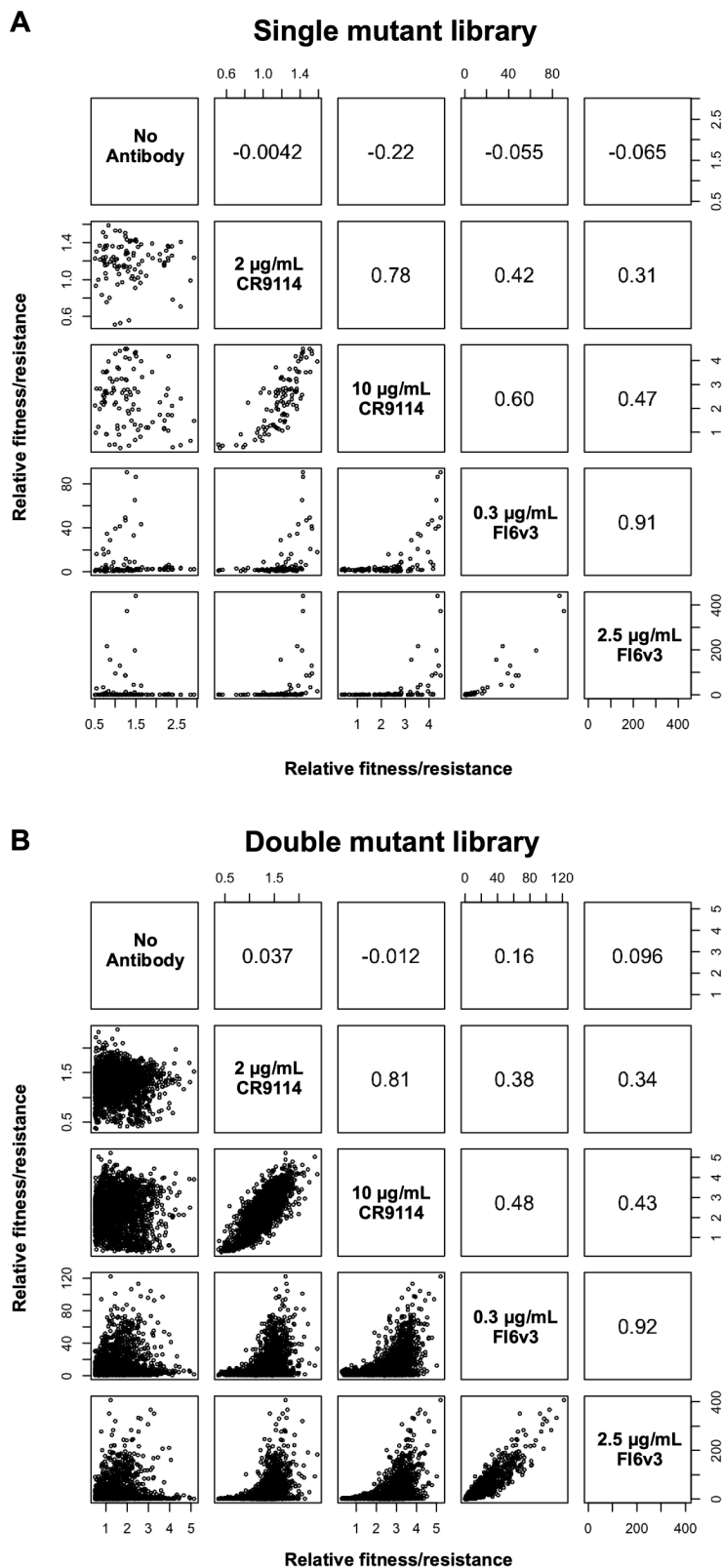
527 Computational scripts for analyzing the H3/HK68 deep mutational scanning data have been
528 deposited to <https://github.com/wchnicholas/HAstemEscape>. Computational scripts for
529 analyzing the H3/Perth09 and H1/WSN deep mutational scanning data have been deposited to
530 https://github.com/bloomlab/HA_stalkbnAb_MAP. Computational scripts for analyzing the
531 CR9114 deep mutational scanning data have been deposited to
532 <https://github.com/wchnicholas/CR9114mut>.



533

534 **Fig. S1. Experimental design and correlation between replicates.** (A) Schematic
 535 representation of the experimental design is shown. (B) Relative fitness of each mutant is
 536 illustrated under different growth conditions. Each data point represents one mutant. Pearson

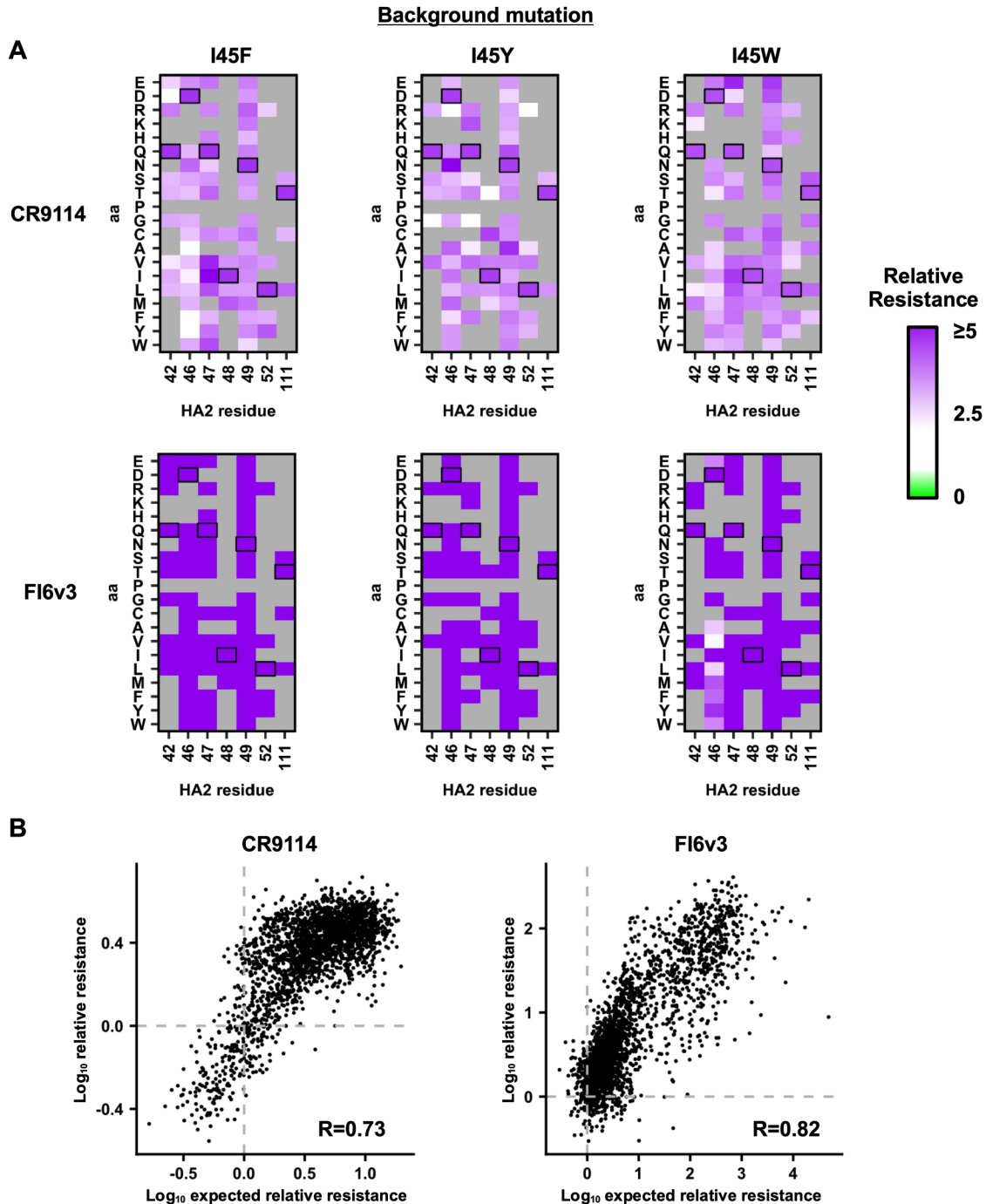
537 correlations (R) of the relative fitness of individual mutants between replicates are shown.
538 Missense variants are colored in purple. Nonsense variants are colored in khaki green. The
539 relative fitness for each mutant correlated well between biological replicates (Pearson
540 correlation = 0.78 to 0.98), thereby demonstrating the high reproducibility of our deep mutational
541 scanning.



542

543 **Fig. S2. Relationships among relative fitness and relative resistance.** The relationships

544 among relative fitness (no antibody), and relative resistance to 2 µg/mL CR9114 antibody, 10
545 µg/mL CR9114 antibody, 0.3 µg/mL FI6v3 antibody, and 2.5 µg/mL FI6v3 antibody for **(A)** single
546 HA mutant virus library, and **(B)** double HA mutant virus library are shown as scatter plots. Each
547 data point in the scatter plots represents a mutant. The Pearson correlation coefficients are
548 indicated. The overall relative resistance profiles between CR9114 and FI6v3 were moderately
549 correlated, as expected given that they target a broadly similar region of the HA. The axes
550 represent relative fitness for “no antibody”, and relative resistance for “2 µg/mL CR9114
551 antibody”, “10 µg/mL CR9114 antibody”, “0.3 µg/mL FI6v3 antibody”, and “2.5 µg/mL FI6v3
552 antibody”.



558 the x/y-axes). For example, the top left data point of the top left heatmap represents the relative
559 resistance of the I45F/Q42E double mutant against 10 µg/mL CR9114 antibody. Relative
560 resistance for WT is set as 1. Virus mutants with a relative fitness of less than 0.5 are excluded
561 from this analysis and are shown as grey. Residues correspond to WT sequence are boxed.
562 When double mutants were composed of at least one strong resistance mutation (e.g. I45F,
563 I45Y, and I45W), they showed strong resistance even if the other mutation did not confer
564 resistance by itself. For example, while most single mutants at residues 47 and 49 did not have
565 high relative resistance (Fig. 2C), mutations at residues 47 or 49 in combination with a mutation
566 with high relative resistance, such as I45Y/F/W, resulted in high relative resistance of the virus
567 to stem bnAbs. **(B)** The relationship of relative resistance of each double mutant to its expected
568 relative resistance calculated from single mutants using an additivity model, where expected
569 relative resistance of double mutant A/B = (relative resistance of single mutant A) × (relative
570 resistance of single mutant B). Pearson correlations (R) between $\log_{10}(\text{relative resistance})$ of
571 each double mutant to its $\log_{10}(\text{expected relative resistance})$ are shown.

A

Human H3N2 isolates that were sequenced without any passaging

Strain	Accession	42	45	46	47	48	49	52	111
A/Virginia/66/2016	EPI_ISL_241581	Q	T	D	Q	I	N	L	T
A/Hawaii/105/2016	EPI_ISL_244700	Q	T	D	Q	I	N	L	T

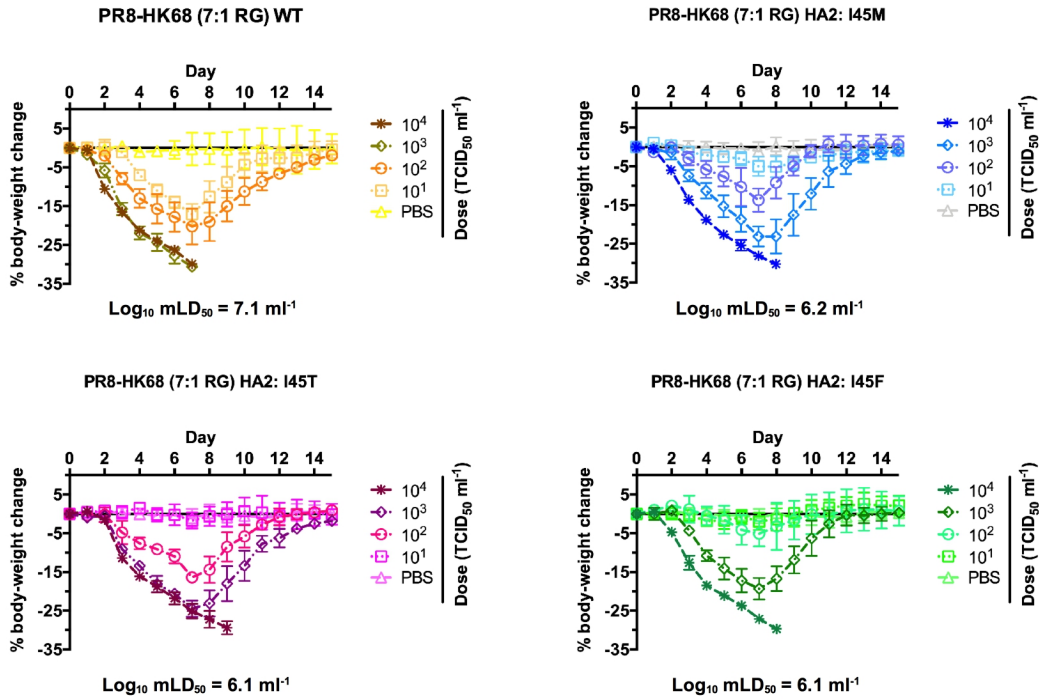
B

Representative strains from different subtypes

Strain	42	45	46	47	48	49	52	111
B/Phuket/3073/2013 (B-Yamagata)	Q	I	N	K	I	T	L	E
B/Brisbane/60/2008 (B-Victoria)	Q	I	N	K	I	T	L	E
A/Hong Kong/3239/2008 (H9)	Q	I	D	K	I	T	V	H
A/turkey/Ontario/6118/1968 (H8)	Q	I	D	K	I	T	V	H
A/duck/Alberta/60/1976 (H12)	Q	I	D	N	M	Q	L	H
A/Taiwan/2/2013 (H6)	Q	I	D	G	I	T	V	H
A/California/04/2009 (H1)	Q	I	D	E	I	T	V	H
A/Japan/305/1957 (H2)	Q	F	D	G	I	T	V	H
A/Vietnam/1203/2004 (H5)	Q	I	D	G	V	T	V	H
A/Duck/England/56 (H11)	Q	I	D	Q	I	T	V	H
A/Gull/Maryland/704/77 (H13)	Q	I	D	Q	I	T	I	H
A/black-headed gull/Sweden/2/99 (H16)	Q	I	N	E	I	T	I	H
A/Brisbane/10/2007 (H3)	Q	I	D	Q	I	N	L	T
A/Duck/Czechoslovakia/1956 (H4)	Q	I	D	Q	I	N	L	T
A/Mallard/Gurijev/263/82 (H14)	Q	I	D	Q	I	N	L	T
A/Jiangxi-Donghu/346/2013 (H10)	Q	I	D	Q	I	T	L	A
A/Shanghai/2/2013 (H7)	Q	I	D	Q	I	T	L	A
A/shearwater/Australia/2576/1979 (H15)	Q	I	D	Q	I	T	L	A

572

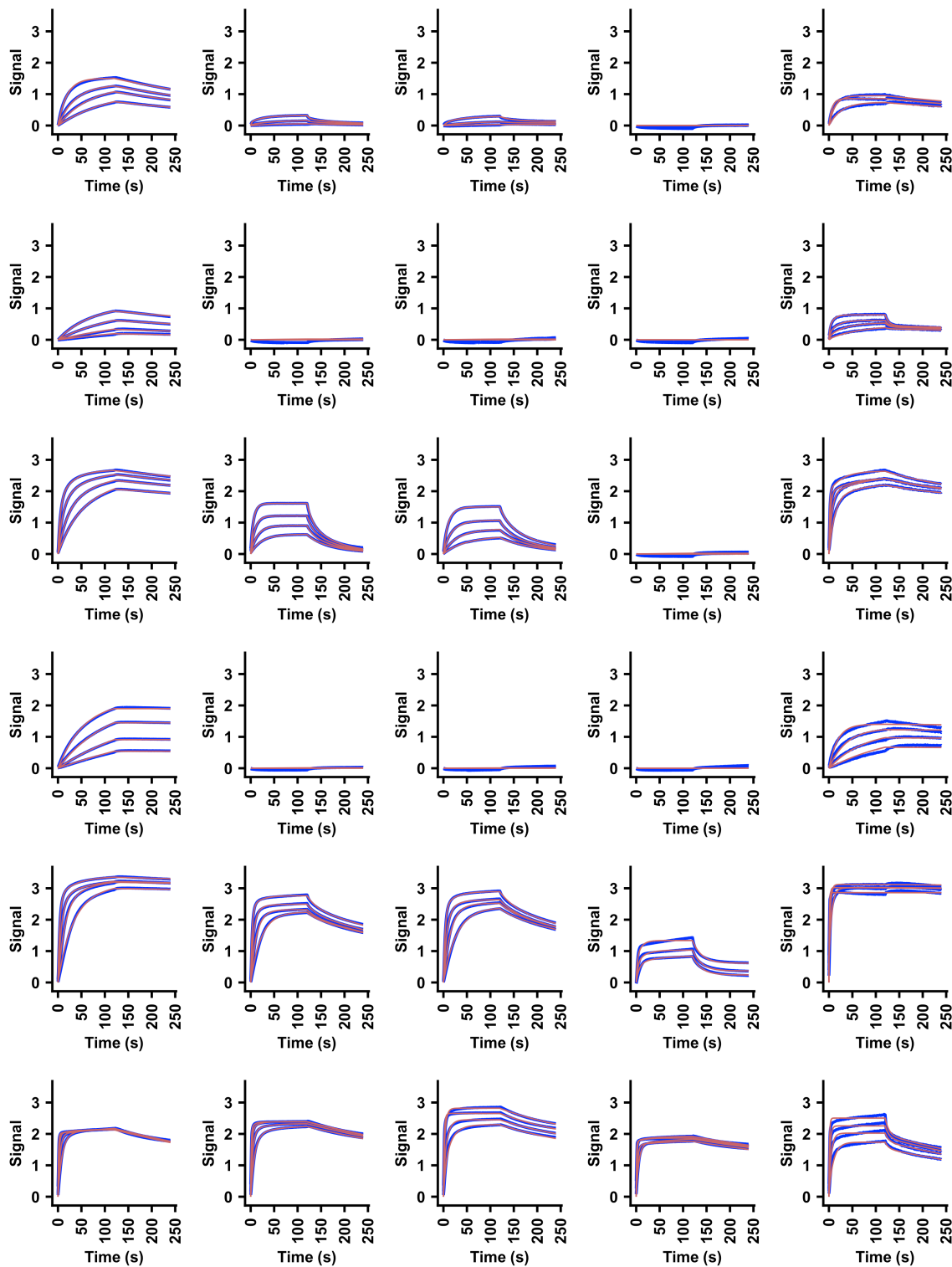
573 **Fig. S4. Sequence alignment of representative influenza strains.** The amino acid variants at
 574 the HA2 residues of interest in **(A)** two human H3N2 isolates that were sequenced without any
 575 passaging and **(B)** representative strains from different HA subtypes and from influenza B virus
 576 are shown.



577

578 **Fig. S5. In vivo pathogenesis of antibody-resistant mutants as determined by weight loss**

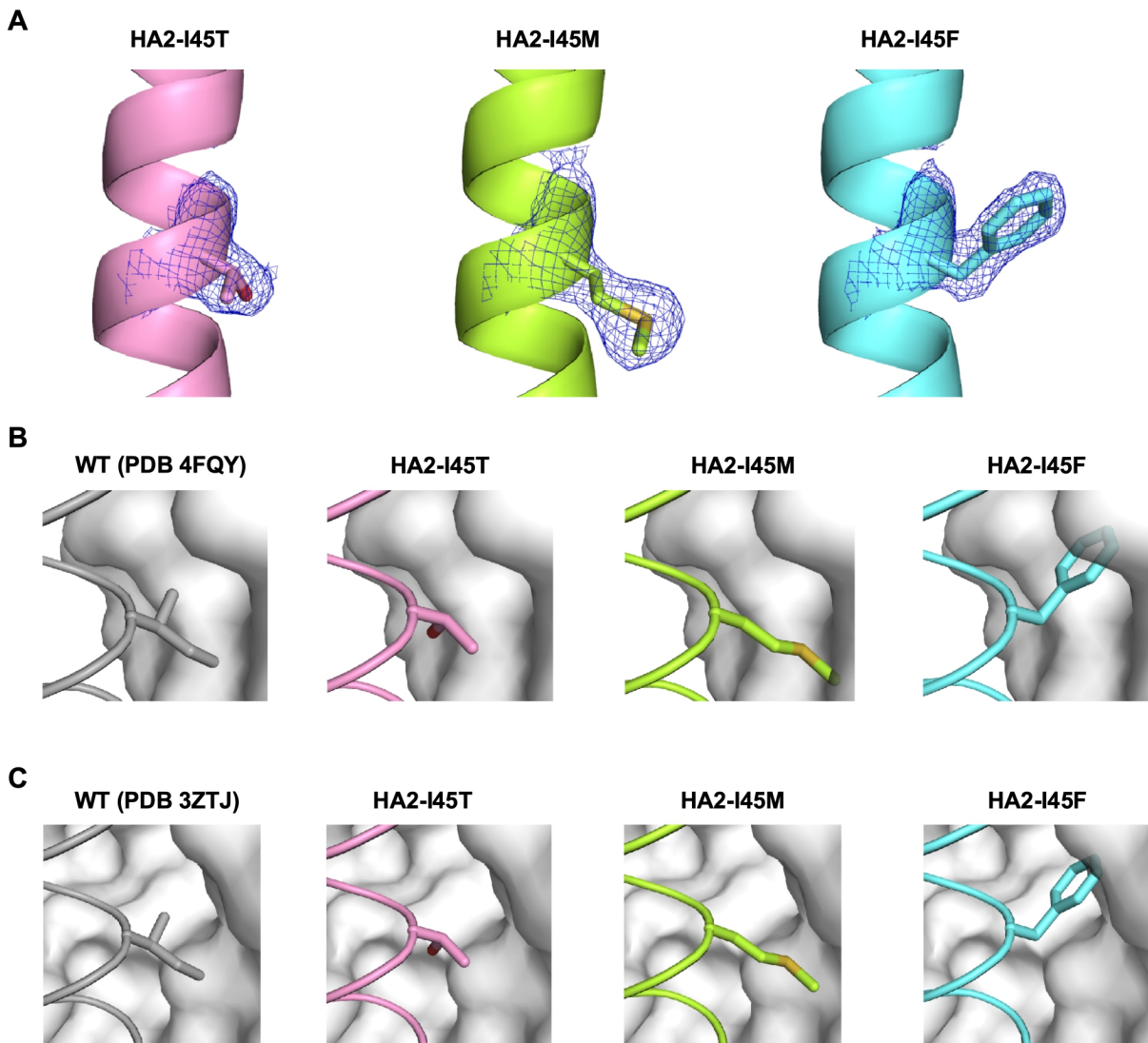
579 **in mice.** Mice were inoculated with the indicated dose ($\text{TCID}_{50} \text{ ml}^{-1}$) of the H3/HK68 (7:1 on
 580 H1/PR8 backbone) WT or mutant viruses. For each dose of WT or mutant viruses, a group of n
 581 = 4 or 5 C57BL/6J mice were used. Body-weight changes were measured. The mean is plotted,
 582 and error bars represent standard deviation. The mLD_{50} for each virus is indicated below the
 583 plots.



584

585 **Fig. S6. Sensorgrams for binding of Fabs and IgGs to HA2 mutants.** Binding kinetics of
586 different Fabs and IgGs against recombinant H3/HK68 HA (WT or mutants) were measured by

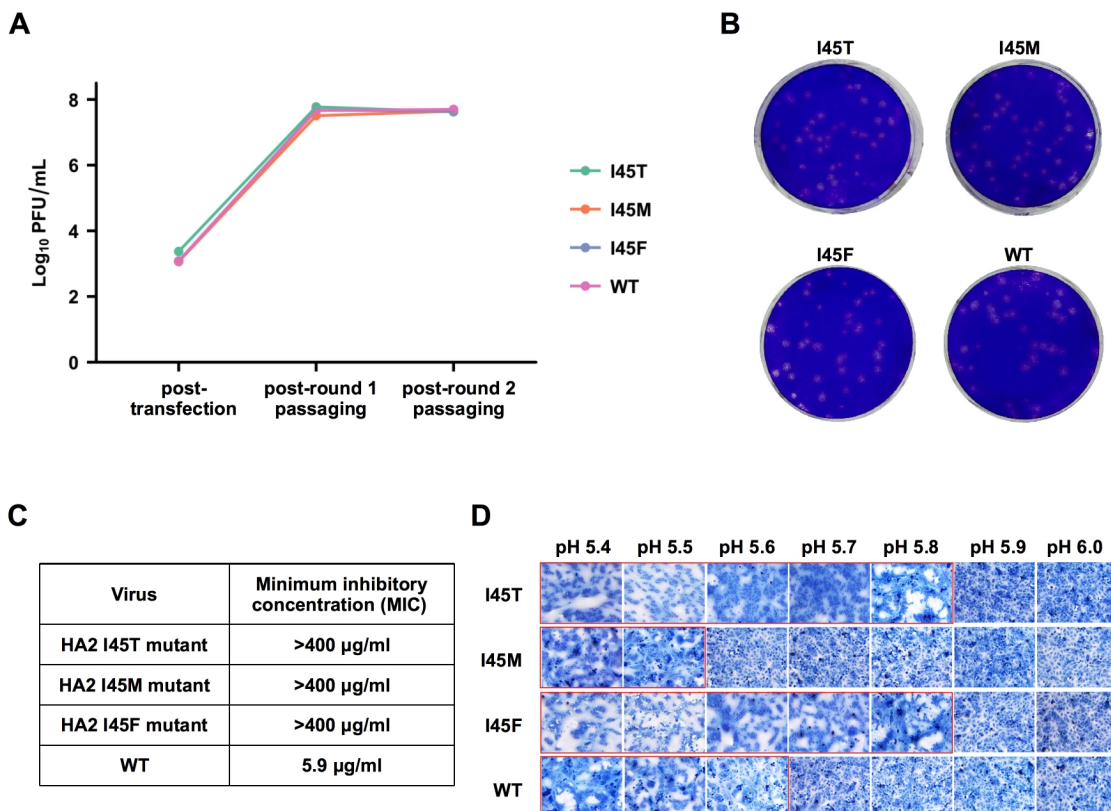
587 biolayer interferometry (BLI). Y-axis represents the response. Blue lines represent the response
588 curve and red lines represent the best fit model (1:1 binding model or 2:1 heterogeneous ligand
589 model, see Methods). Binding kinetics were measured for three to four concentrations of Fab at
590 2-fold dilution ranging from 1,000 nM to 125 nM. Of note, the bivalence of IgG can significantly
591 enhance its binding as compared to Fab. Such an observation has been described in our
592 previous study of stem bnAb 27F3 (34).



593

594 **Fig. S7. Structural characterization of H3/HK68 HA2 mutants.** (A) Final 2Fo-Fc electron
 595 density maps for HA2 residue 45 in different mutants are represented in a blue mesh and
 596 contoured at 1.0 σ . The side chains of HA2 residue 45 in different mutants are shown in stick
 597 representation. (B) To analyze the effect of different HA2 mutants on CR9114 binding, the apo
 598 structures of HA2 I45T, I45M, and I45F mutants were aligned with WT H3/HK68 HA in complex
 599 with CR9114 Fab (PDB 4FQY) (26). The backbone of helix A is shown in tube representation,
 600 side chain of residue 45 in stick representation, and CR9114 Fab in surface representation. (C)
 601 To analyze the effect of different HA2 mutants on Fl6v3 binding, the apo structures of HA2 I45T,

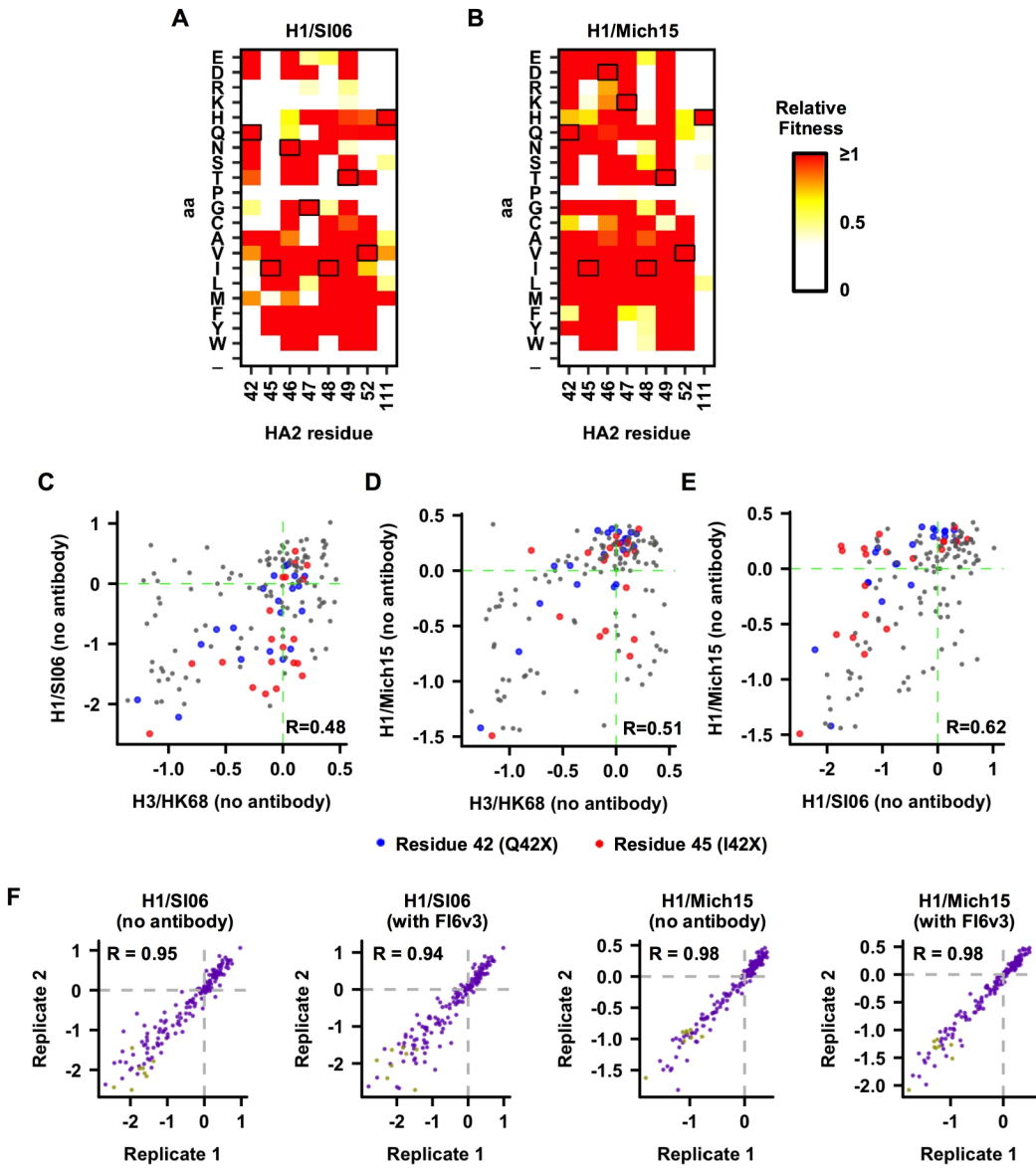
602 I45M, and I45F mutants are aligned with the WT H3/HK68 HA in complex with FI6v3 Fab (PDB
603 3ZTJ) (27). The backbone of helix A is shown in tube representation, the side chain of residue
604 45 in stick representation, and FI6v3 Fab in surface representation.



605

606 **Fig. S8. Characterization of A/Wuhan/359/95 (H3N2) HA2 mutants.** **(A)** Recombinant viruses
 607 were rescued at 293T cells and then passaged in MDCK cells at an MOI of 0.001 PFU/cell (for
 608 round 1 passaging) or 0.005 PFU/cell (for round 2 passaging). The titer for viral rescue (post-
 609 transfection) and post-passaging is shown. **(B)** Plaque morphologies of A/Wuhan/359/95
 610 (H3/Wuhan95) HA2 mutants are shown. **(C)** The minimum inhibitory concentrations (MIC) of
 611 Fl6v3 to H3/Wuhan95 HA2 mutants I45T, I45M, I45F, and wild type (WT) are shown. **(D)** The pH
 612 for HA activation was determined by syncytium formation in Vero cells after infection with
 613 recombinant H3/Wuhan95 viruses at an MOI of 10. Representative images (x10 magnification)
 614 of syncytium formation at indicated pH values are shown. The experiments were repeated twice
 615 with recombinant viruses after one passage in MDCK cells and once with recombinant viruses
 616 after two passages in MDCK cells. The fusion pHs of H3/Wuhan95 I45T, I45M, and I45F were
 617 pH 5.8, 5.5, and 5.8, respectively, which differed slightly from pH 5.6 of WT. Increase in fusion

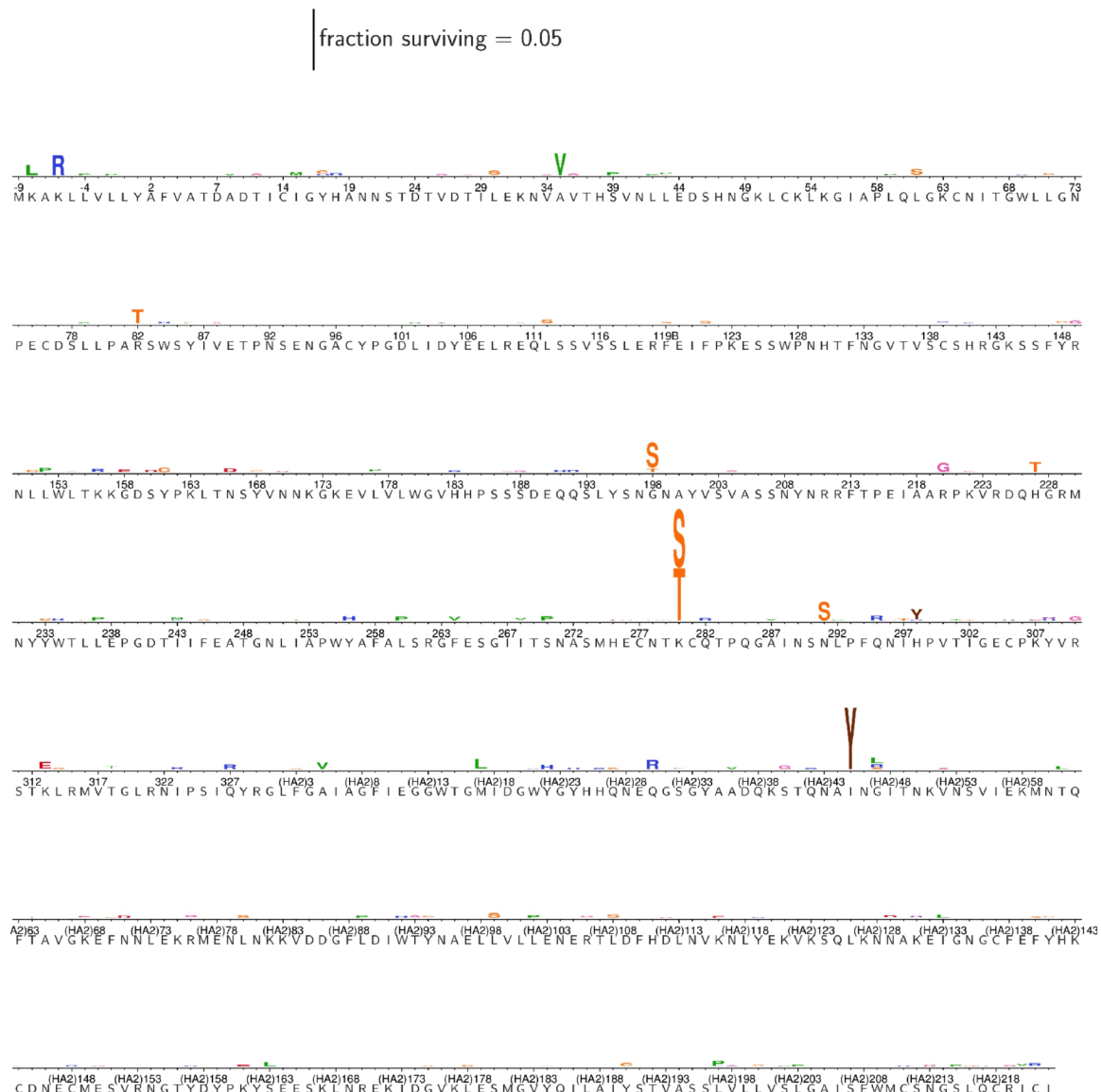
618 pH can contribute to resistance against HA stem bnAbs (21, 68, 69).



619

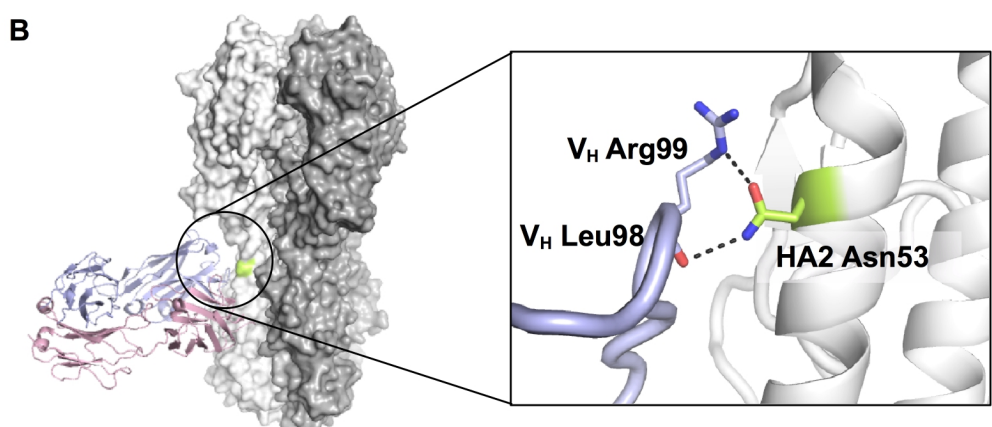
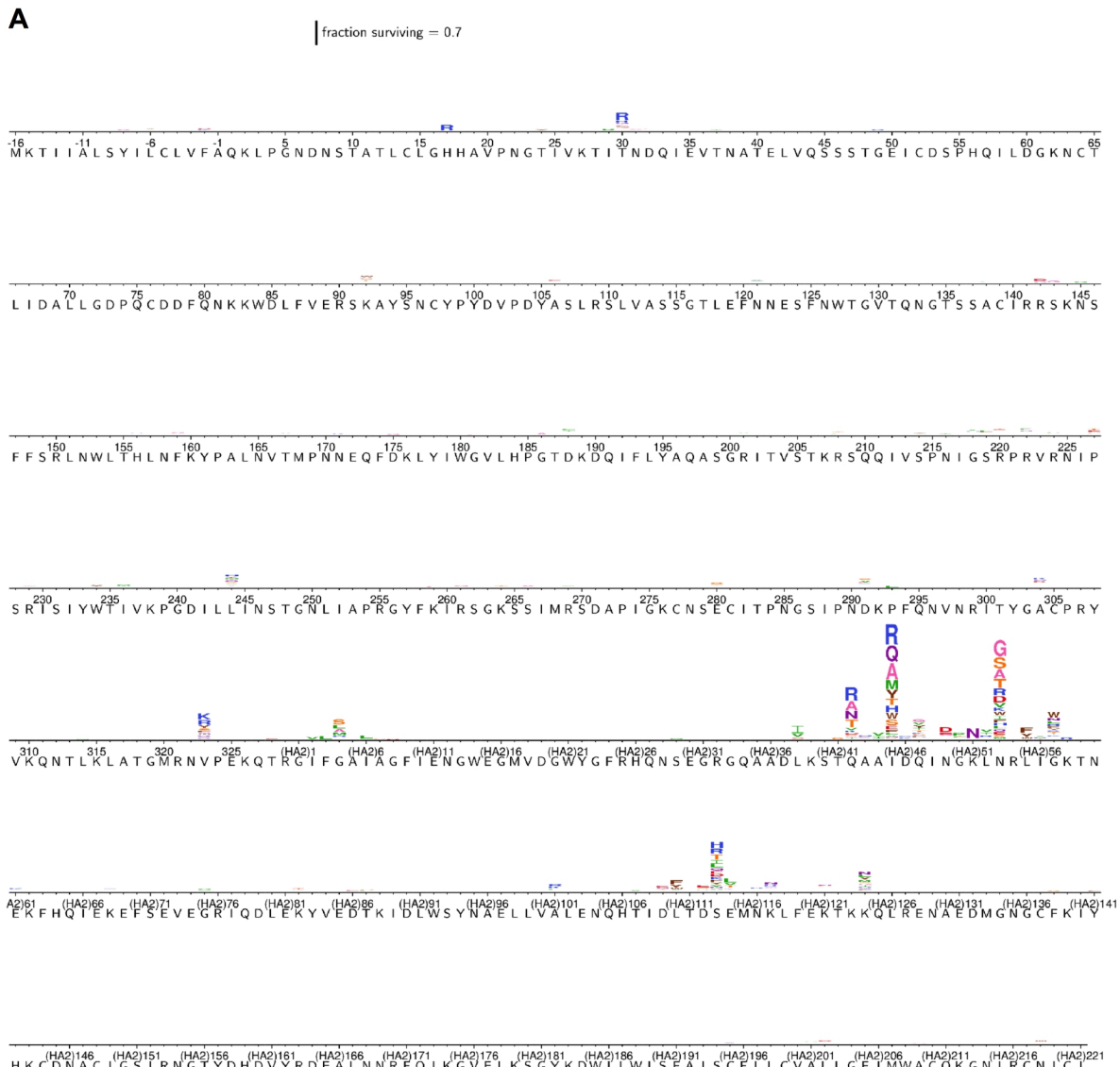
620 **Fig. S9. HA stem mutational fitness profiles of H1/SI06 and H1/Mich15.** (A-B) Based on the
 621 deep mutational scanning experiment, relative fitness of single mutants in (A) H1/SI06, and (B)
 622 H1/Mich15 viruses are shown. Relative fitness of wild type (WT) is set as 1. Residues
 623 corresponding to WT sequence are boxed. (C-E) The \log_{10} relative fitness of each single
 624 mutation in HA2 residues 42, 45, 46, 47, 48, 49, 52, and 111 of H3/HK68, H1/SI06, and
 625 H1/Mich15 in the absence of antibody are compared. (C) H3/HK68 vs H1/SI06. (D) H3/HK68 vs
 626 H1/Mich15. (E) H1/SI06 vs H1/Mich15. Each data point represents one mutant. Data points that

627 represent mutations at residues 42 and 45 are colored in blue and red, respectively. Data points
628 that represent mutations at other residues are colored in grey. Pearson correlation (R) is shown.
629 These plots aim to analyze whether a given mutation has a similar fitness effect in different
630 strains. For example, if a mutation that has a high fitness in one strain generally has a high
631 fitness in another strain, a high correlation will be observed. **(F)** Relative fitness of each mutant
632 in H1/SI06 and H1/Mich15 under different growth conditions is shown. Each data point
633 represents one mutant. Pearson correlations (R) of the relative fitness of individual mutants
634 between replicates are shown. Missense variants are colored in purple. Nonsense variants are
635 colored in khaki green. The fitness measurements for each mutant in H1/SI06 and H1/Mich15
636 correlate well between biological replicates, demonstrating a high reproducibility of the results.



637

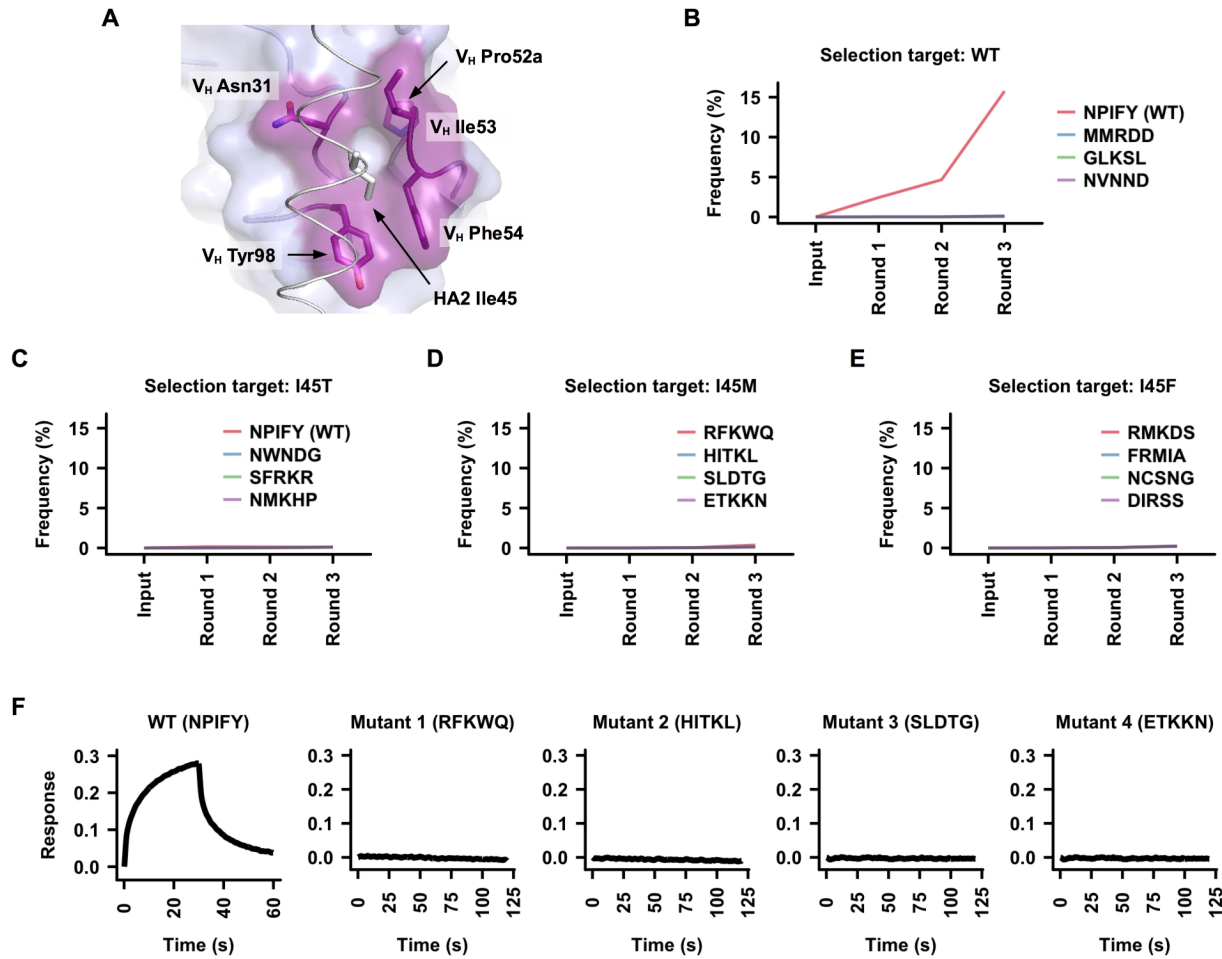
638 **Fig. S10. The excess fraction surviving selection with bnAb CR9114 for all amino-acid**
 639 **mutations in H1/WSN HA.** The height of each letter is proportional to the excess fraction of
 640 virion surviving with that mutation. The scale bar at the top of the plot relates the letter heights to
 641 the actual fractions. The sites are labeled using H3 numbering.



642

643 **Fig. S11. The excess fraction surviving selection with bnAb Fl6v3 for all amino-acid**

644 **mutations in H3/Perth09 HA. (A)** The height of each letter is proportional to the excess fraction
645 of virion surviving with that mutation. The scale bar at the top of the plot relates the letter heights
646 to the actual fractions. The sites are labeled using H3 numbering. **(B)** HA2 Asn53 forms a
647 hydrogen bond with the side chain of Fl6v3 V_H Arg99 as well as with the main-chain carbonyl of
648 Fl6v3 V_H Leu98 (PDB 3ZTJ) (1). Fl6v3 heavy chain is shown in blue, Fl6v3 light chain in pink,
649 and HA2 Asn53 in lime. Hydrogen bonds are represented by black dashed lines.



650

651 **Fig. S12. An attempt to overcome resistance mutations by evolving CR9114.** We attempted
 652 to evolve CR9114 to bind to CR9114-resistance HA2 mutants using saturation mutagenesis and
 653 yeast display selection. **(A)** When CR9114 binds to HA, HA2-Ile45 is surrounded by multiple V_H
 654 residues, including Asn31, Pro52a, Ile53, Phe54, and Tyr98. Saturation mutagenesis was
 655 performed at these five V_H residues to generate a total of 3.2 million CR9114 variants ($20^5 =$
 656 3,200,000). These CR9114 variants were displayed on the yeast surface in a Fab format (59)
 657 and underwent three rounds of selections against WT or mutant H3/HK68 HA. **(B-E)** The
 658 change in frequencies during the selection process were shown for: **(B)** the top four variants in
 659 post three-round selection against WT, **(C)** the top four CR9114 variants in post three-round
 660 selection against HA2-I45T mutant, **(D)** the top four CR9114 variants in post three-round

661 selection against HA2-I45M mutant, and (E) the top four CR9114 variants in post three-round
662 selection against HA2-I45F mutant. During the selection against WT H3/HK68 HA, the variant
663 represents the WT CR9114 (NPIFY, abbreviated after the amino acids at the five residues of
664 interest) was readily enriched. In contrast, none of the CR9114 variants showed significant
665 enrichment during selections against those three HA2 mutants. This observation suggests that
666 we failed to identify any variant from the mutant library that could overcome those three
667 resistance HA2 mutants (I45T, I45M, and I45F). (F) The top four CR9114 variants in post three-
668 round selection against HA2-I45M mutant, along with WT CR9114, were individually expressed
669 and tested binding against recombinant HA2-I45M mutant. At 1 μ M concentration, none of the
670 CR9114 variants exhibited any binding to the recombinant HA2-I45M mutant, whereas WT
671 CR9114 showed weak binding at the same concentration. This result demonstrates that it might
672 be difficult to overcome those resistance mutants by simply introducing amino-acid substitutions
673 in the bnAb.

Table S1. X-ray data collection and refinement statistics

Data collection	H3/HK68 HA2-I45M	H3/HK68 HA2-I45T	H3/HK68 HA2-I45F
Beamline	SSRL 12-2	SSRL 12-2	SSRL 12-2
Wavelength (Å)	0.9795	0.9795	0.9795
Space group	C2	C2	C2
Unit cell parameters (Å and °)	a=208.9, b=131.0, c=72.6, β=98.4	a=209.2, b=131.1, c=72.2, β=98.1	a=208.4, b=131.4, c=72.3, β=98.1
Resolution (Å)	50-2.50 (2.60-2.50) ^a	50-2.25 (2.35-2.25) ^a	50-2.10 (2.20-2.10) ^a
Unique reflections	65,790 (7,333) ^a	89,621 (10,991) ^a	110,282 (13,871) ^a
Redundancy	5.9 (5.9) ^a	5.0 (4.7) ^a	5.6 (5.2) ^a
Completeness (%)	97.6 (98.4) ^a	97.4 (95.7) ^a	97.4 (98.1) ^a
<I/σ _I >	15.4 (1.5) ^a	16.2 (1.3) ^a	20.0 (1.7) ^a
R _{sym} ^b	0.12 (0.87) ^a	0.09 (0.94) ^a	0.10 (0.83) ^a
R _{pim} ^b	0.05 (0.39) ^a	0.04 (0.49) ^a	0.05 (0.40) ^a
CC _{1/2} ^c	1.00 (0.70) ^a	1.00 (0.68) ^a	1.00 (0.77) ^a
Z _a ^d	3	3	3
Refinement statistics			
Resolution (Å)	50-2.50	50-2.25	50-2.10
Reflections (work)	61,835	84,488	103,850
Reflections (test)	3,292	4,390	5,420
R _{cryst} (%) ^e / R _{free} (%) ^f	19.0 / 21.9	18.2 / 20.8	18.4 / 21.6
No. of atoms			
Protein	11,526	11,517	11,546
Water	321	666	846
Glycan	318	332	332
Average B-value (Å ²)			
Protein	57	50	48
Water	44	46	48
Glycan	88	79	71
Wilson B-value (Å ²)	48	38	32
RMSD from ideal geometry			
Bond length (Å)	0.011	0.011	0.011
Bond angle (°)	1.52	1.55	1.50
Ramachandran statistics (%)^g			
Favored	96.5	97.1	97.1
Outliers	0.2	0.2	0.2
PDB code	6NHQ	6NHP	6NHR

^a Numbers in parentheses refer to the highest resolution shell.

^b R_{sym} = $\sum_{hkl} \sum_i |I_{hkl,i} - \langle I_{hkl} \rangle| / \sum_{hkl} \sum_i I_{hkl,i}$ and R_{pim} = $\sum_{hkl} (1/(n-1))^{1/2} \sum_i |I_{hkl,i} - \langle I_{hkl} \rangle| / \sum_{hkl} \sum_i I_{hkl,i}$, where I_{hkl,i} is the scaled intensity of the ith measurement of reflection h, k, l, $\langle I_{hkl} \rangle$ is the average intensity for that reflection, and n is the redundancy.

^c CC_{1/2} = Pearson correlation coefficient between two random half datasets.

^d Z_a is the number of HA protomers per crystallographic asymmetric unit.

^e R_{cryst} = $\sum_{hkl} |F_o - F_c| / \sum_{hkl} |F_o| \times 100$, where F_o and F_c are the observed and calculated structure factors,

^f R_{free} was calculated as for R_{cryst}, but on a test set comprising 5% of the data excluded from refinement.

^g Calculated with MolProbity (64).

Table S2. Primers for construction of H3/HK68 mutant libraries

StemLib-VF	5'-CGT ACG TCT CAA GTG CTT TTA AGA TCT GCT GCT TGT-3'
StemLib-VR	5'-CGT ACG TCT CAT CGG AAA TGA ACA AGC TGT TTG AGA-3'
StemLib-WT-R	5'-CGT ACG TCT CAC CGA GTC AGT CAG GTC AAT TGT ATG TTG ATT CT-3'
StemLib-WT-F	5'-ACG TCT CAC ACT CAA GCA GCC ATC GAC CAA ATC AAT GGG AAA TTG AAC AGG GTA ATC GAG-3'
StemLib-111-R	5'-CGT ACG TCT CAC CGA ATC SNN CAG GTC AAT TGT ATG TTG ATT CT-3'
StemLib-42-F	5'-ACG TCT CAC ACT NNK GCC GCA ATC GAC CAA ATC AAT GGA AAA TTG AAC AGG GTA ATC GAG-3'
StemLib-45-F	5'-ACG TCT CAC ACT CAA GCC GCA NNK GAC CAA ATC AAT GGC AAA TTG AAC AGG GTA ATC GAG-3'
StemLib-46-F	5'-ACG TCT CAC ACT CAA GCC GCA ATC NNK CAA ATC AAT GGT AAA TTG AAC AGG GTA ATC GAG-3'
StemLib-47-F	5'-ACG TCT CAC ACT CAA GCC GCT ATC GAC NNK ATC AAT GGA AAA TTG AAC AGG GTA ATC GAG-3'
StemLib-48-F	5'-ACG TCT CAC ACT CAA GCC GCT ATC GAC CAA NNK AAT GGC AAA TTG AAC AGG GTA ATC GAG-3'
StemLib-49-F	5'-ACG TCT CAC ACT CAA GCC GCT ATC GAC CAA ATC NNS GGT AAA TTG AAC AGG GTA ATC GAG-3'
StemLib-52-F	5'-ACG TCT CAC ACT CAA GCC GCG ATC GAC CAA ATC AAT GGA AAA NNK AAC AGG GTA ATC GAG-3'
StemLib-42/45-F	5'-ACG TCT CAC ACT NNK GCC GCG NNK GAC CAA ATC AAT GGC AAA TTG AAC AGG GTA ATC GAG-3'
StemLib-42/46-F	5'-ACG TCT CAC ACT NNK GCC GCG ATC NNK CAA ATC AAT GGT AAA TTG AAC AGG GTA ATC GAG-3'
StemLib-42/47-F	5'-ACG TCT CAC ACT NNK GCT GCA ATC GAC NNK ATC AAT GGA AAA TTG AAC AGG GTA ATC GAG-3'
StemLib-42/48-F	5'-ACG TCT CAC ACT NNK GCT GCA ATC GAC CAA NNK AAT GGC AAA TTG AAC AGG GTA ATC GAG-3'
StemLib-42/49-F	5'-ACG TCT CAC ACT NNK GCT GCA ATC GAC CAA ATC NNS GGT AAA TTG AAC AGG GTA ATC GAG-3'
StemLib-42/52-F	5'-ACG TCT CAC ACT NNK GCT GCT ATC GAC CAA ATC AAT GGA AAA NNK AAC AGG GTA ATC GAG-3'
StemLib-45/46-F	5'-ACG TCT CAC ACT CAA GCT GCT NNK CAA ATC AAT GGC AAA TTG AAC AGG GTA ATC GAG-3'
StemLib-45/47-F	5'-ACG TCT CAC ACT CAA GCT GCT NNK GAC NNK ATC AAT GGT AAA TTG AAC AGG GTA ATC GAG-3'
StemLib-45/48-F	5'-ACG TCT CAC ACT CAA GCT GCG NNK GAC CAA NNK AAT GGA AAA TTG AAC AGG GTA ATC GAG-3'
StemLib-45/49-F	5'-ACG TCT CAC ACT CAA GCT GCG NNK GAC CAA ATC NNS GGC AAA TTG AAC AGG GTA ATC GAG-3'
StemLib-45/52-F	5'-ACG TCT CAC ACT CAA GCT GCG NNK GAC CAA ATC AAT GGT AAA NNK AAC AGG GTA ATC GAG-3'
StemLib-46/47-F	5'-ACG TCT CAC ACT CAA GCG GCA ATC NNK NNK ATC AAT GGA AAA TTG AAC AGG GTA ATC GAG-3'
StemLib-46/48-F	5'-ACG TCT CAC ACT CAA GCG GCA ATC NNK CAA NNK AAT GGC AAA TTG AAC AGG GTA ATC GAG-3'
StemLib-46/49-F	5'-ACG TCT CAC ACT CAA GCG GCA ATC NNK CAA ATC NNS GGT AAA TTG AAC AGG GTA ATC GAG-3'
StemLib-46/52-F	5'-ACG TCT CAC ACT CAA GCG GCT ATC NNK CAA ATC AAT GGA AAA NNK AAC AGG GTA ATC GAG-3'
StemLib-47/48-F	5'-ACG TCT CAC ACT CAA GCG GCT ATC GAC NNK NNK AAT GGC AAA TTG AAC AGG GTA ATC GAG-3'
StemLib-47/49-F	5'-ACG TCT CAC ACT CAA GCG GCT ATC GAC NNK ATC NNS GGT AAA TTG AAC AGG GTA ATC GAG-3'
StemLib-47/52-F	5'-ACG TCT CAC ACT CAA GCG GCG ATC GAC NNK ATC AAT GGA AAA NNK AAC AGG GTA ATC GAG-3'
StemLib-48/49-F	5'-ACG TCT CAC ACT CAA GCG GCG ATC GAC CAA NNK NNS GGC AAA TTG AAC AGG GTA ATC GAG-3'
StemLib-48/52-F	5'-ACG TCT CAC ACT CAA GCG GCG ATC GAC CAA NNK AAT GGT AAA NNK AAC AGG GTA ATC GAG-3'
StemLib-49/52-F	5'-ACG TCT CAC ACT CAA GCA GCA ATC GAC CAA ATC NNS GGA AAA NNK AAC AGG GTA ATC GAG-3'

677

Table S3. Primers for construction of H1/SI06 and H1/Mich15 mutant libraries

H1/SI06	StemLib-VF	5'-CGT ACG TCT CAT CAA ATG TGA AGA ATC TGT ATG AGA-3'
	StemLib-VR	5'-CGT ACG TCT CAT GTG CTT TTT TGG TCC GCA GCA TAG-3'
	StemLib-WT-F	5'-ACG TCT CAC ACA CAA AAT GCC ATT AAC GGG ATT ACA AAC AAG GTG AAT TCT GTA ATC GAG-3'
	StemLib-42-F	5'-ACG TCT CAC ACA CAA AAT GCC ATT AAC GGG ATT ACA AAC AAG GTG AAT TCT GTA ATC GAG-3'
	StemLib-45-F	5'-ACG TCT CAC ACA CAA AAT GCC NNS AAC GGG ATT ACA AAC AAG GTG AAT TCT GTA ATC GAG-3'
	StemLib-46-F	5'-ACG TCT CAC ACA CAA AAT GCC ATT NNK GGG ATT ACA AAC AAG GTG AAT TCT GTA ATC GAG-3'
	StemLib-47-F	5'-ACG TCT CAC ACA CAA AAT GCC ATT AAC NNK ATT ACA AAC AAG GTG AAT TCT GTA ATC GAG-3'
	StemLib-48-F	5'-ACG TCT CAC ACA CAA AAT GCC ATT AAC GGG NNS ACA AAC AAG GTG AAT TCT GTA ATC GAG-3'
	StemLib-49-F	5'-ACG TCT CAC ACA CAA AAT GCC ATT AAC GGG ATT NNK AAC AAG GTG AAT TCT GTA ATC GAG-3'
	StemLib-52-F	5'-ACG TCT CAC ACA CAA AAT GCC ATT AAC GGG ATT ACA AAC AAG NNK ATT TCT GTA ATC GAG-3'
	StemLib-WT-R	5'-CGT ACG TCT CAT TGA GTC ATG AAA ATC CAA AGT CCT CTC ATT TT-3'
	StemLib-111-R	5'-CGT ACG TCT CAT TGA GTC SNN AAA ATC CAA AGT CCT CTC ATT TT-3'
H1/Mich15	StemLib-VF	5'-CGT ACG TCT CAT CAA ATG TGA AGA ACT TGT ATG AAA-3'
	StemLib-VR	5'-CGT ACG TCT CAT GTG CTC TTC AGG TCG GCT GCA TAT-3'
	StemLib-WT-F	5'-ACG TCT CAC ACA CAA AAT GCC ATT GAC AAG ATT ACT AAC AAA GTA AAT TCT GTT ATT GAA-3'
	StemLib-42-F	5'-ACG TCT CAC ACA NNK AAT GCC ATT GAC AAG ATT ACT AAC AAA GTA AAT TCT GTT ATT GAA-3'
	StemLib-45-F	5'-ACG TCT CAC ACA CAA AAT GCC NNS GAC AAG ATT ACT AAC AAA GTA AAT TCT GTT ATT GAA-3'
	StemLib-46-F	5'-ACG TCT CAC ACA CAA AAT GCC ATT NNK AAG ATT ACT AAC AAA GTA AAT TCT GTT ATT GAA-3'
	StemLib-47-F	5'-ACG TCT CAC ACA CAA AAT GCC ATT GAC NNK ATT ACT AAC AAA GTA AAT TCT GTT ATT GAA-3'
	StemLib-48-F	5'-ACG TCT CAC ACA CAA AAT GCC ATT GAC AAG NNS ACT AAC AAA GTA AAT TCT GTT ATT GAA-3'
	StemLib-49-F	5'-ACG TCT CAC ACA CAA AAT GCC ATT GAC AAG ATT NNS AAC AAA GTA AAT TCT GTT ATT GAA-3'
	StemLib-52-F	5'-ACG TCT CAC ACA CAA AAT GCC ATT GAC AAG ATT ACT AAC AAA NNK ATT TCT GTT ATT GAA-3'
	StemLib-WT-R	5'-CGT ACG TCT CAT TGA ATC GTG ATA GTC CAA AGT TCT TTC ATT TT-3'
	StemLib-111-R	5'-CGT ACG TCT CAT TGA ATC SNN ATA GTC CAA AGT TCT TTC ATT TT-3'

678

679

References and Notes

1. I. A. Wilson, J. J. Skehel, D. C. Wiley, Structure of the haemagglutinin membrane glycoprotein of influenza virus at 3 Å resolution. *Nature* **289**, 366–373 (1981). [doi:10.1038/289366a0](https://doi.org/10.1038/289366a0) [Medline](#)
2. D. C. Wiley, I. A. Wilson, J. J. Skehel, Structural identification of the antibody-binding sites of Hong Kong influenza haemagglutinin and their involvement in antigenic variation. *Nature* **289**, 373–378 (1981). [doi:10.1038/289373a0](https://doi.org/10.1038/289373a0) [Medline](#)
3. A. J. Caton, G. G. Brownlee, J. W. Yewdell, W. Gerhard, The antigenic structure of the influenza virus A/PR/8/34 hemagglutinin (H1 subtype). *Cell* **31**, 417–427 (1982). [doi:10.1016/0092-8674\(82\)90135-0](https://doi.org/10.1016/0092-8674(82)90135-0) [Medline](#)
4. F. Krammer, P. Palese, Advances in the development of influenza virus vaccines. *Nat. Rev. Drug Discov.* **14**, 167–182 (2015). [doi:10.1038/nrd4529](https://doi.org/10.1038/nrd4529) [Medline](#)
5. N. C. Wu, I. A. Wilson, A perspective on the structural and functional constraints for immune evasion: Insights from influenza virus. *J. Mol. Biol.* **429**, 2694–2709 (2017). [doi:10.1016/j.jmb.2017.06.015](https://doi.org/10.1016/j.jmb.2017.06.015) [Medline](#)
6. M. Throsby, E. van den Brink, M. Jongeneelen, L. L. M. Poon, P. Alard, L. Cornelissen, A. Bakker, F. Cox, E. van Deventer, Y. Guan, J. Cinatl, J. ter Meulen, I. Lasters, R. Carsetti, M. Peiris, J. de Kruif, J. Goudsmit, Heterosubtypic neutralizing monoclonal antibodies cross-protective against H5N1 and H1N1 recovered from human IgM⁺ memory B cells. *PLOS ONE* **3**, e3942 (2008). [doi:10.1371/journal.pone.0003942](https://doi.org/10.1371/journal.pone.0003942) [Medline](#)
7. J. Sui, W. C. Hwang, S. Perez, G. Wei, D. Aird, L. M. Chen, E. Santelli, B. Stec, G. Cadwell, M. Ali, H. Wan, A. Murakami, A. Yammanuru, T. Han, N. J. Cox, L. A. Bankston, R. O. Donis, R. C. Liddington, W. A. Marasco, Structural and functional bases for broad-spectrum neutralization of avian and human influenza A viruses. *Nat. Struct. Mol. Biol.* **16**, 265–273 (2009). [doi:10.1038/nsmb.1566](https://doi.org/10.1038/nsmb.1566) [Medline](#)
8. N. C. Wu, I. A. Wilson, Structural insights into the design of novel anti-influenza therapies. *Nat. Struct. Mol. Biol.* **25**, 115–121 (2018). [doi:10.1038/s41594-018-0025-9](https://doi.org/10.1038/s41594-018-0025-9) [Medline](#)
9. D. C. Ekiert, G. Bhabha, M.-A. Elsiger, R. H. E. Friesen, M. Jongeneelen, M. Throsby, J. Goudsmit, I. A. Wilson, Antibody recognition of a highly conserved influenza virus epitope. *Science* **324**, 246–251 (2009). [doi:10.1126/science.1171491](https://doi.org/10.1126/science.1171491) [Medline](#)
10. A. Impagliazzo, F. Milder, H. Kuipers, M. V. Wagner, X. Zhu, R. M. B. Hoffman, R. van Meersbergen, J. Huizingh, P. Wanningen, J. Verspuij, M. de Man, Z. Ding, A. Apetri, B. Kükrer, E. Sneekes-Vriese, D. Tomkiewicz, N. S. Laursen, P. S. Lee, A. Zakrzewska, L. Dekking, J. Tolboom, L. Tettero, S. van Meerten, W. Yu, W. Koudstaal, J. Goudsmit, A. B. Ward, W. Meijberg, I. A. Wilson, K. Radošević, A stable trimeric influenza hemagglutinin stem as a broadly protective immunogen. *Science* **349**, 1301–1306 (2015). [doi:10.1126/science.aac7263](https://doi.org/10.1126/science.aac7263) [Medline](#)
11. H. M. Yassine, J. C. Boyington, P. M. McTamney, C.-J. Wei, M. Kanekiyo, W.-P. Kong, J. R. Gallagher, L. Wang, Y. Zhang, M. G. Joyce, D. Lingwood, S. M. Moin, H. Andersen, Y. Okuno, S. S. Rao, A. K. Harris, P. D. Kwong, J. R. Mascola, G. J. Nabel, B. S.

- Graham, Hemagglutinin-stem nanoparticles generate heterosubtypic influenza protection. *Nat. Med.* **21**, 1065–1070 (2015). [doi:10.1038/nm.3927](https://doi.org/10.1038/nm.3927) [Medline](#)
12. S. A. Valkenburg, V. V. A. Mallajosyula, O. T. W. Li, A. W. H. Chin, G. Carnell, N. Temperton, R. Varadarajan, L. L. M. Poon, Stalking influenza by vaccination with pre-fusion headless HA mini-stem. *Sci. Rep.* **6**, 22666 (2016). [doi:10.1038/srep22666](https://doi.org/10.1038/srep22666) [Medline](#)
 13. K. S. Corbett, S. M. Moin, H. M. Yassine, A. Cagigi, M. Kanekiyo, S. Boyoglu-Barnum, S. I. Myers, Y. Tsybovsky, A. K. Wheatley, C. A. Schramm, R. A. Gillespie, W. Shi, L. Wang, Y. Zhang, S. F. Andrews, M. G. Joyce, M. C. Crank, D. C. Douek, A. B. McDermott, J. R. Mascola, B. S. Graham, J. C. Boyington, Design of nanoparticulate group 2 influenza virus hemagglutinin stem antigens that activate unmutated ancestor B cell receptors of broadly neutralizing antibody lineages. *mBio* **10**, e02810–e02818 (2019). [doi:10.1128/mBio.02810-18](https://doi.org/10.1128/mBio.02810-18) [Medline](#)
 14. S. J. Fleishman, T. A. Whitehead, D. C. Ekiert, C. Dreyfus, J. E. Corn, E.-M. Strauch, I. A. Wilson, D. Baker, Computational design of proteins targeting the conserved stem region of influenza hemagglutinin. *Science* **332**, 816–821 (2011). [doi:10.1126/science.1202617](https://doi.org/10.1126/science.1202617) [Medline](#)
 15. T. A. Whitehead, A. Chevalier, Y. Song, C. Dreyfus, S. J. Fleishman, C. De Mattos, C. A. Myers, H. Kamisetty, P. Blair, I. A. Wilson, D. Baker, Optimization of affinity, specificity and function of designed influenza inhibitors using deep sequencing. *Nat. Biotechnol.* **30**, 543–548 (2012). [doi:10.1038/nbt.2214](https://doi.org/10.1038/nbt.2214) [Medline](#)
 16. A. Chevalier, D.-A. Silva, G. J. Rocklin, D. R. Hicks, R. Vergara, P. Murapa, S. M. Bernard, L. Zhang, K.-H. Lam, G. Yao, C. D. Bahl, S.-I. Miyashita, I. Goreshnik, J. T. Fuller, M. T. Koday, C. M. Jenkins, T. Colvin, L. Carter, A. Bohn, C. M. Bryan, D. A. Fernández-Velasco, L. Stewart, M. Dong, X. Huang, R. Jin, I. A. Wilson, D. H. Fuller, D. Baker, Massively parallel de novo protein design for targeted therapeutics. *Nature* **550**, 74–79 (2017). [doi:10.1038/nature23912](https://doi.org/10.1038/nature23912) [Medline](#)
 17. R. U. Kadam, J. Juraszek, B. Brandenburg, C. Buyck, W. B. G. Schepens, B. Kesteleyn, B. Stoops, R. J. Vreeken, J. Vermond, W. Goutier, C. Tang, R. Vogels, R. H. E. Friesen, J. Goudsmit, M. J. P. van Dongen, I. A. Wilson, Potent peptidic fusion inhibitors of influenza virus. *Science* **358**, 496–502 (2017). [doi:10.1126/science.aan0516](https://doi.org/10.1126/science.aan0516) [Medline](#)
 18. M. J. P. van Dongen, R. U. Kadam, J. Juraszek, E. Lawson, B. Brandenburg, F. Schmitz, W. B. G. Schepens, B. Stoops, H. A. van Diepen, M. Jongeneelen, C. Tang, J. Vermond, A. van Eijgen-Obregoso Real, S. Blokland, D. Garg, W. Yu, W. Goutier, E. Lanckacker, J. M. Klap, D. C. G. Peeters, J. Wu, C. Buyck, T. H. M. Jonckers, D. Roymans, P. Roevens, R. Vogels, W. Koudstaal, R. H. E. Friesen, P. Raboisson, D. Dhanak, J. Goudsmit, I. A. Wilson, A small-molecule fusion inhibitor of influenza virus is orally active in mice. *Science* **363**, eaar6221 (2019). [doi:10.1126/science.aar6221](https://doi.org/10.1126/science.aar6221) [Medline](#)
 19. E. Sparrow, M. Friede, M. Sheikh, S. Torvaldsen, A. T. Newall, Passive immunization for influenza through antibody therapies, a review of the pipeline, challenges and potential applications. *Vaccine* **34**, 5442–5448 (2016). [doi:10.1016/j.vaccine.2016.08.057](https://doi.org/10.1016/j.vaccine.2016.08.057) [Medline](#)
 20. G. Nakamura, N. Chai, S. Park, N. Chiang, Z. Lin, H. Chiu, R. Fong, D. Yan, J. Kim, J. Zhang, W. P. Lee, A. Estevez, M. Coons, M. Xu, P. Lupardus, M. Balazs, L. R. Swem,

An in vivo human-plasmablast enrichment technique allows rapid identification of therapeutic influenza A antibodies. *Cell Host Microbe* **14**, 93–103 (2013).
[doi:10.1016/j.chom.2013.06.004](https://doi.org/10.1016/j.chom.2013.06.004) [Medline](#)

21. N. Chai, L. R. Swem, M. Reichelt, H. Chen-Harris, E. Luis, S. Park, A. Fouts, P. Lupardus, T. D. Wu, O. Li, J. McBride, M. Lawrence, M. Xu, M.-W. Tan, Two escape mechanisms of influenza A virus to a broadly neutralizing stalk-binding antibody. *PLOS Pathog.* **12**, e1005702 (2016). [doi:10.1371/journal.ppat.1005702](https://doi.org/10.1371/journal.ppat.1005702) [Medline](#)
22. C. S. Anderson, S. Ortega, F. A. Chaves, A. M. Clark, H. Yang, D. J. Topham, M. L. DeDiego, Natural and directed antigenic drift of the H1 influenza virus hemagglutinin stalk domain. *Sci. Rep.* **7**, 14614 (2017). [doi:10.1038/s41598-017-14931-7](https://doi.org/10.1038/s41598-017-14931-7) [Medline](#)
23. M. B. Doud, J. M. Lee, J. D. Bloom, How single mutations affect viral escape from broad and narrow antibodies to H1 influenza hemagglutinin. *Nat. Commun.* **9**, 1386 (2018). [doi:10.1038/s41467-018-03665-3](https://doi.org/10.1038/s41467-018-03665-3) [Medline](#)
24. D. M. Fowler, S. Fields, Deep mutational scanning: A new style of protein science. *Nat. Methods* **11**, 801–807 (2014). [doi:10.1038/nmeth.3027](https://doi.org/10.1038/nmeth.3027) [Medline](#)
25. R. H. Friesen, P. S. Lee, E. J. M. Stoop, R. M. B. Hoffman, D. C. Ekiert, G. Bhabha, W. Yu, J. Juraszek, W. Koudstaal, M. Jongeneelen, H. J. W. M. Korse, C. Ophorst, E. C. M. Brinkman-van der Linden, M. Throsby, M. J. Kwakkenbos, A. Q. Bakker, T. Beaumont, H. Spits, T. Kwaks, R. Vogels, A. B. Ward, J. Goudsmit, I. A. Wilson, A common solution to group 2 influenza virus neutralization. *Proc. Natl. Acad. Sci. U.S.A.* **111**, 445–450 (2014). [doi:10.1073/pnas.1319058110](https://doi.org/10.1073/pnas.1319058110) [Medline](#)
26. C. Dreyfus, N. S. Laursen, T. Kwaks, D. Zuidgeest, R. Khayat, D. C. Ekiert, J. H. Lee, Z. Metlagel, M. V. Bujny, M. Jongeneelen, R. van der Vlugt, M. Lamrani, H. J. W. M. Korse, E. Geelen, Ö. Sahin, M. Sieuwerts, J. P. J. Brakenhoff, R. Vogels, O. T. W. Li, L. L. M. Poon, M. Peiris, W. Koudstaal, A. B. Ward, I. A. Wilson, J. Goudsmit, R. H. E. Friesen, Highly conserved protective epitopes on influenza B viruses. *Science* **337**, 1343–1348 (2012). [doi:10.1126/science.1222908](https://doi.org/10.1126/science.1222908) [Medline](#)
27. D. Corti, J. Voss, S. J. Gamblin, G. Codoni, A. Macagno, D. Jarrossay, S. G. Vachieri, D. Pinna, A. Minola, F. Vanzetta, C. Silacci, B. M. Fernandez-Rodriguez, G. Agatic, S. Bianchi, I. Giacchett-Sasselli, L. Calder, F. Sallusto, P. Collins, L. F. Haire, N. Temperton, J. P. M. Langedijk, J. J. Skehel, A. Lanzavecchia, A neutralizing antibody selected from plasma cells that binds to group 1 and group 2 influenza A hemagglutinins. *Science* **333**, 850–856 (2011). [doi:10.1126/science.1205669](https://doi.org/10.1126/science.1205669) [Medline](#)
28. N. C. Wu, A. P. Young, L. Q. Al-Mawsawi, C. A. Olson, J. Feng, H. Qi, S.-H. Chen, I.-H. Lu, C.-Y. Lin, R. G. Chin, H. H. Luan, N. Nguyen, S. F. Nelson, X. Li, T.-T. Wu, R. Sun, High-throughput profiling of influenza A virus hemagglutinin gene at single-nucleotide resolution. *Sci. Rep.* **4**, 4942 (2014). [doi:10.1038/srep04942](https://doi.org/10.1038/srep04942) [Medline](#)
29. B. Thyagarajan, J. D. Bloom, The inherent mutational tolerance and antigenic evolvability of influenza hemagglutinin. *eLife* **3**, e03300 (2014). [doi:10.7554/eLife.03300](https://doi.org/10.7554/eLife.03300) [Medline](#)
30. N. C. Wu, J. Xie, T. Zheng, C. M. Nycholat, G. Grande, J. C. Paulson, R. A. Lerner, I. A. Wilson, Diversity of functionally permissive sequences in the receptor-binding site of

- influenza hemagglutinin. *Cell Host Microbe* **21**, 742–753.e8 (2017). [doi:10.1016/j.chom.2017.05.011](https://doi.org/10.1016/j.chom.2017.05.011) [Medline](#)
31. M. B. Doud, S. E. Hensley, J. D. Bloom, Complete mapping of viral escape from neutralizing antibodies. *PLOS Pathog.* **13**, e1006271 (2017). [doi:10.1371/journal.ppat.1006271](https://doi.org/10.1371/journal.ppat.1006271) [Medline](#)
32. R. B. Squires, J. Noronha, V. Hunt, A. García-Sastre, C. Macken, N. Baumgarth, D. Suarez, B. E. Pickett, Y. Zhang, C. N. Larsen, A. Ramsey, L. Zhou, S. Zaremba, S. Kumar, J. Deitrich, E. Klem, R. H. Scheuermann, Influenza research database: An integrated bioinformatics resource for influenza research and surveillance. *Influenza Other Respir. Viruses* **6**, 404–416 (2012). [doi:10.1111/j.1750-2659.2011.00331.x](https://doi.org/10.1111/j.1750-2659.2011.00331.x) [Medline](#)
33. N. C. Wu, S. J. Zost, A. J. Thompson, D. Oyen, C. M. Nycholat, R. McBride, J. C. Paulson, S. E. Hensley, I. A. Wilson, A structural explanation for the low effectiveness of the seasonal influenza H3N2 vaccine. *PLOS Pathog.* **13**, e1006682 (2017). [doi:10.1371/journal.ppat.1006682](https://doi.org/10.1371/journal.ppat.1006682) [Medline](#)
34. S. Lang, J. Xie, X. Zhu, N. C. Wu, R. A. Lerner, I. A. Wilson, Antibody 27F3 broadly targets influenza A group 1 and 2 hemagglutinins through a further variation in V_H1-69 antibody orientation on the HA stem. *Cell Rep.* **20**, 2935–2943 (2017). [doi:10.1016/j.celrep.2017.08.084](https://doi.org/10.1016/j.celrep.2017.08.084) [Medline](#)
35. R. Yoshida, M. Igarashi, H. Ozaki, N. Kishida, D. Tomabechi, H. Kida, K. Ito, A. Takada, Cross-protective potential of a novel monoclonal antibody directed against antigenic site B of the hemagglutinin of influenza A viruses. *PLOS Pathog.* **5**, e1000350 (2009). [doi:10.1371/journal.ppat.1000350](https://doi.org/10.1371/journal.ppat.1000350) [Medline](#)
36. P. S. Lee, R. Yoshida, D. C. Ekiert, N. Sakai, Y. Suzuki, A. Takada, I. A. Wilson, Heterosubtypic antibody recognition of the influenza virus hemagglutinin receptor binding site enhanced by avidity. *Proc. Natl. Acad. Sci. U.S.A.* **109**, 17040–17045 (2012). [doi:10.1073/pnas.1212371109](https://doi.org/10.1073/pnas.1212371109) [Medline](#)
37. M. B. Doud, J. D. Bloom, Accurate measurement of the effects of all amino-acid mutations on influenza hemagglutinin. *Viruses* **8**, 155 (2016). [doi:10.3390/v8060155](https://doi.org/10.3390/v8060155) [Medline](#)
38. J. M. Lee, J. Huddleston, M. B. Doud, K. A. Hooper, N. C. Wu, T. Bedford, J. D. Bloom, Deep mutational scanning of hemagglutinin helps predict evolutionary fates of human H3N2 influenza variants. *Proc. Natl. Acad. Sci. U.S.A.* **115**, E8276–E8285 (2018). [doi:10.1073/pnas.1806133115](https://doi.org/10.1073/pnas.1806133115) [Medline](#)
39. Kabat numbering scheme is commonly used standard for numbering the amino-acid residues in an antibody. Third complementarity-determining region of heavy chain (CDR H3) ranges from residues 95 to 102 in the Kabat numbering scheme. Residues inserted in CDR H3 are numbered with 100a, 100b, 100c, and so on.
40. S. J. Zost, N. C. Wu, S. E. Hensley, I. A. Wilson, Immunodominance and antigenic variation of influenza virus hemagglutinin: Implications for design of universal vaccine immunogens. *J. Infect. Dis.* **219** (suppl. 1), S38–S45 (2019). [doi:10.1093/infdis/jiy696](https://doi.org/10.1093/infdis/jiy696) [Medline](#)
41. D. C. Ekiert, R. H. E. Friesen, G. Bhabha, T. Kwaks, M. Jongeneelen, W. Yu, C. Ophorst, F. Cox, H. J. W. M. Korse, B. Brandenburg, R. Vogels, J. P. J. Brakenhoff, R. Kompier, M.

- H. Koldijk, L. A. H. M. Cornelissen, L. L. M. Poon, M. Peiris, W. Koudstaal, I. A. Wilson, J. Goudsmit, A highly conserved neutralizing epitope on group 2 influenza A viruses. *Science* **333**, 843–850 (2011). [doi:10.1126/science.1204839](https://doi.org/10.1126/science.1204839) [Medline](#)
42. E. Kirkpatrick, X. Qiu, P. C. Wilson, J. Bahl, F. Krammer, The influenza virus hemagglutinin head evolves faster than the stalk domain. *Sci. Rep.* **8**, 10432 (2018). [doi:10.1038/s41598-018-28706-1](https://doi.org/10.1038/s41598-018-28706-1) [Medline](#)
43. M. G. Joyce, A. K. Wheatley, P. V. Thomas, G.-Y. Chuang, C. Soto, R. T. Bailer, A. Druz, I. S. Georgiev, R. A. Gillespie, M. Kanekiyo, W.-P. Kong, K. Leung, S. N. Narpala, M. S. Prabhakaran, E. S. Yang, B. Zhang, Y. Zhang, M. Asokan, J. C. Boyington, T. Bylund, S. Darko, C. R. Lees, A. Ransier, C.-H. Shen, L. Wang, J. R. Whittle, X. Wu, H. M. Yassine, C. Santos, Y. Matsuoka, Y. Tsybovsky, U. Baxa, J. C. Mullikin, K. Subbarao, D. C. Douek, B. S. Graham, R. A. Koup, J. E. Ledgerwood, M. Roederer, L. Shapiro, P. D. Kwong, J. R. Mascola, A. B. McDermott; NISC Comparative Sequencing Program, Vaccine-induced antibodies that neutralize group 1 and group 2 influenza A viruses. *Cell* **166**, 609–623 (2016). [doi:10.1016/j.cell.2016.06.043](https://doi.org/10.1016/j.cell.2016.06.043) [Medline](#)
44. Y. Okuno, Y. Isegawa, F. Sasao, S. Ueda, A common neutralizing epitope conserved between the hemagglutinins of influenza A virus H1 and H2 strains. *J. Virol.* **67**, 2552–2558 (1993). [doi:10.1128/JVI.67.5.2552-2558.1993](https://doi.org/10.1128/JVI.67.5.2552-2558.1993) [Medline](#)
45. C. Dreyfus, D. C. Ekiert, I. A. Wilson, Structure of a classical broadly neutralizing stem antibody in complex with a pandemic H2 influenza virus hemagglutinin. *J. Virol.* **87**, 7149–7154 (2013). [doi:10.1128/JVI.02975-12](https://doi.org/10.1128/JVI.02975-12) [Medline](#)
46. N. L. Kallewaard, D. Corti, P. J. Collins, U. Neu, J. M. McAuliffe, E. Benjamin, L. Wachter-Rosati, F. J. Palmer-Hill, A. Q. Yuan, P. A. Walker, M. K. Vorlaender, S. Bianchi, B. Guarino, A. De Marco, F. Vanzetta, G. Agatic, M. Foglierini, D. Pinna, B. Fernandez-Rodriguez, A. Fruehwirth, C. Silacci, R. W. Ogrodnowicz, S. R. Martin, F. Sallusto, J. A. A. Suzich, A. Lanzavecchia, Q. Zhu, S. J. Gamblin, J. J. Skehel, Structure and function analysis of an antibody recognizing all influenza A subtypes. *Cell* **166**, 596–608 (2016). [doi:10.1016/j.cell.2016.05.073](https://doi.org/10.1016/j.cell.2016.05.073) [Medline](#)
47. J. Lee, J. Bloom, jbloomlab/HA_stalkbnAb_MAP: journal submission, Version journal_submission, Zenodo (9 February 2020); <https://doi.org/10.5281/zenodo.3660467>.
48. N. C. Wu, wchnicholas/HAstemEscape: publication, Version publication, Zenodo (9 February 2020); <https://doi.org/10.5281/zenodo.3660739>.
49. N. C. Wu, wchnicholas/CR9114mut: publication, Version publication, Zenodo (9 February 2020); <https://doi.org/10.5281/zenodo.3660731>.
50. G. Neumann, T. Watanabe, H. Ito, S. Watanabe, H. Goto, P. Gao, M. Hughes, D. R. Perez, R. Donis, E. Hoffmann, G. Hobom, Y. Kawaoka, Generation of influenza A viruses entirely from cloned cDNAs. *Proc. Natl. Acad. Sci. U.S.A.* **96**, 9345–9350 (1999). [doi:10.1073/pnas.96.16.9345](https://doi.org/10.1073/pnas.96.16.9345) [Medline](#)
51. E. Hoffmann, G. Neumann, Y. Kawaoka, G. Hobom, R. G. Webster, A DNA transfection system for generation of influenza A virus from eight plasmids. *Proc. Natl. Acad. Sci. U.S.A.* **97**, 6108–6113 (2000). [doi:10.1073/pnas.100133697](https://doi.org/10.1073/pnas.100133697) [Medline](#)

52. H. L. Yen, L. M. Herlocher, E. Hoffmann, M. N. Matrosovich, A. S. Monto, R. G. Webster, E. A. Govorkova, Neuraminidase inhibitor-resistant influenza viruses may differ substantially in fitness and transmissibility. *Antimicrob. Agents Chemother.* **49**, 4075–4084 (2005). [doi:10.1128/AAC.49.10.4075-4084.2005](https://doi.org/10.1128/AAC.49.10.4075-4084.2005) Medline
53. C. A. Olson, N. C. Wu, R. Sun, A comprehensive biophysical description of pairwise epistasis throughout an entire protein domain. *Curr. Biol.* **24**, 2643–2651 (2014). [doi:10.1016/j.cub.2014.09.072](https://doi.org/10.1016/j.cub.2014.09.072) Medline
54. J. D. Bloom, Software for the analysis and visualization of deep mutational scanning data. *BMC Bioinformatics* **16**, 168 (2015). [doi:10.1186/s12859-015-0590-4](https://doi.org/10.1186/s12859-015-0590-4) Medline
55. K. Katoh, D. M. Standley, MAFFT multiple sequence alignment software version 7: Improvements in performance and usability. *Mol. Biol. Evol.* **30**, 772–780 (2013). [doi:10.1093/molbev/mst010](https://doi.org/10.1093/molbev/mst010) Medline
56. C. D. McWhite, A. G. Meyer, C. O. Wilke, Sequence amplification via cell passaging creates spurious signals of positive adaptation in influenza virus H3N2 hemagglutinin. *Virus Evol.* **2**, vew026 (2016). [doi:10.1093/ve/vew026](https://doi.org/10.1093/ve/vew026) Medline
57. G. E. Crooks, G. Hon, J. M. Chandonia, S. E. Brenner, WebLogo: A sequence logo generator. *Genome Res.* **14**, 1188–1190 (2004). [doi:10.1101/gr.849004](https://doi.org/10.1101/gr.849004) Medline
58. D. C. Ekiert, A. K. Kashyap, J. Steel, A. Rubrum, G. Bhabha, R. Khayat, J. H. Lee, M. A. Dillon, R. E. O’Neil, A. M. Faynboym, M. Horowitz, L. Horowitz, A. B. Ward, P. Palese, R. Webby, R. A. Lerner, R. R. Bhatt, I. A. Wilson, Cross-neutralization of influenza A viruses mediated by a single antibody loop. *Nature* **489**, 526–532 (2012). [doi:10.1038/nature11414](https://doi.org/10.1038/nature11414) Medline
59. N. C. Wu, G. Grande, H. L. Turner, A. B. Ward, J. Xie, R. A. Lerner, I. A. Wilson, In vitro evolution of an influenza broadly neutralizing antibody is modulated by hemagglutinin receptor specificity. *Nat. Commun.* **8**, 15371 (2017). [doi:10.1038/ncomms15371](https://doi.org/10.1038/ncomms15371) Medline
60. Z. Otwinowski, W. Minor, Processing of x-ray diffraction data collected in oscillation mode. *Methods Enzymol.* **276**, 307–326 (1997). [doi:10.1016/S0076-6879\(97\)76066-X](https://doi.org/10.1016/S0076-6879(97)76066-X)
61. A. J. McCoy, R. W. Grosse-Kunstleve, P. D. Adams, M. D. Winn, L. C. Storoni, R. J. Read, Phaser crystallographic software. *J. Appl. Crystallogr.* **40**, 658–674 (2007). [doi:10.1107/S0021889807021206](https://doi.org/10.1107/S0021889807021206) Medline
62. P. Emsley, B. Lohkamp, W. G. Scott, K. Cowtan, Features and development of Coot. *Acta Crystallogr. D Biol. Crystallogr.* **66**, 486–501 (2010). [doi:10.1107/S0907444910007493](https://doi.org/10.1107/S0907444910007493) Medline
63. G. N. Murshudov, P. Skubák, A. A. Lebedev, N. S. Pannu, R. A. Steiner, R. A. Nicholls, M. D. Winn, F. Long, A. A. Vagin, REFMAC5 for the refinement of macromolecular crystal structures. *Acta Crystallogr. D Biol. Crystallogr.* **67**, 355–367 (2011). [doi:10.1107/S0907444911001314](https://doi.org/10.1107/S0907444911001314) Medline
64. V. B. Chen, W. B. Arendall 3rd, J. J. Headd, D. A. Keedy, R. M. Immormino, G. J. Kapral, L. W. Murray, J. S. Richardson, D. C. Richardson, MolProbity: All-atom structure validation for macromolecular crystallography. *Acta Crystallogr. D Biol. Crystallogr.* **66**, 12–21 (2010). [doi:10.1107/S0907444909042073](https://doi.org/10.1107/S0907444909042073) Medline

65. W. Kabsch, C. Sander, Dictionary of protein secondary structure: Pattern recognition of hydrogen-bonded and geometrical features. *Biopolymers* **22**, 2577–2637 (1983).
[doi:10.1002/bip.360221211](https://doi.org/10.1002/bip.360221211) [Medline](#)
66. M. Z. Tien, A. G. Meyer, D. K. Sydykova, S. J. Spielman, C. O. Wilke, Maximum allowed solvent accessibilites of residues in proteins. *PLOS ONE* **8**, e80635 (2013).
[doi:10.1371/journal.pone.0080635](https://doi.org/10.1371/journal.pone.0080635) [Medline](#)
67. L. Benatuil, J. M. Perez, J. Belk, C. M. Hsieh, An improved yeast transformation method for the generation of very large human antibody libraries. *Protein Eng. Des. Sel.* **23**, 155–159 (2010). [doi:10.1093/protein/gzq002](https://doi.org/10.1093/protein/gzq002) [Medline](#)
68. S. Yamayoshi, A. Yasuhara, M. Ito, R. Uraki, Y. Kawaoka, Differences in the ease with which mutant viruses escape from human monoclonal antibodies against the HA stem of influenza A virus. *J. Clin. Virol.* **108**, 105–111 (2018). [doi:10.1016/j.jcv.2018.09.016](https://doi.org/10.1016/j.jcv.2018.09.016) [Medline](#)
69. N. C. Wu, S. Yamayoshi, M. Ito, R. Uraki, Y. Kawaoka, I. A. Wilson, Recurring and adaptable binding motifs in broadly neutralizing antibodies to influenza virus are encoded on the D3-9 segment of the Ig gene. *Cell Host Microbe* **24**, 569–578.e4 (2018).
[doi:10.1016/j.chom.2018.09.010](https://doi.org/10.1016/j.chom.2018.09.010) [Medline](#)